MENOUFIA JOURNAL OF SOIL SCIENCE

https://mjss.journals.ekb.eg

SOIL ORIGIN AND UNIFORMITY IN DAM-CONTROLLED WATERSHEDS ACROSS WADI EL-MADAMUDE USING PEDOLOGICAL AND GEOELECTRICAL MEASUREMENTS, EAST LUXOR, EGYPT.

Elwan, A. A.[(1)*] and Barseem, M.S. M.[(2)]

[(1)] Pedology Department, Desert Research Center, 1st Mathaf El-Matariya, 11753, Cairo, Egypt

[(2)] Geophysical Exploration Department, Desert Research Center, 1st Mathaf El-Matariya, 11753, Egypt

Received: Sep. 14 , 2023 Accepted: Sep. 28 , 2023

ABSTRACT: Traditional soil science methods for estimating spatial changes in soil parameters within any farm are time-consuming and do not allow for the measurement of short-term variability. Geophysical approaches provide a high-accuracy alternative to typical soil sampling methods. The primary goal was to assess the appropriateness of measuring soil apparent electrical resistivity (Rho; ρ) as geoelectrical technique for mapping and predicting soil attributes linked to soil origin and uniformity in Wadi El-Madamude, east Luxor, Upper Egypt. The relationships were performed among Rho and soil morphological, physical, chemical, mineralogical, and geochemical properties. The electrical resistance of obtained soil samples by genetic horizons was measured in the laboratory using a resistivity Ohm.m meter. The soils of Wadi El-Madamude were classified into four reference soil groups based on the W.R.B. system namely: Leptosols, Regosols, Calcisols, and Solonchaks. The following are the horizonation sequences of the examined soil groups from upstream to downstream of Wadi El-Madamude: C-Cr-R was assigned to Leptosols, C-Ck-2Cm-Cr to Regosols, Ap-Bk-2Ck1-2Ck2 to Calcisols, and Ap-Bw-Btkz- Btkm-Btm-Btg-W to Solonchaks. The Rho values ranged wildly horizontally across Wadi El-Madamude and vertically within the soil pedon. Clay soils of Solonchaks have lower resistivity values than sandy soils of Leptosols and Regosols. Leptosols have the highest values (70129.3-98120.5 Ω m), Regosols (13546.1-59147.5 Ω m), Calcisols (7126.3-21357.2 Ω m), and Solonchaks (55.1-73.2 Ω m). The soils were evaluated for their origin and uniformity based on mineralogical and geochemical studies and indices. Upper Wadi El-Madamude sediments are derived from limestone and high-grade metamorphic rocks. In contrast, downstream soils are derived from fine Nile floodplain products and recent coarse deposits from the upland (midstream and upstream). Within the soil pedons of Regosols and Calcisols, lithological discontinuities were discovered. The homogeneity of the soil was determined using the uniformity value and the C.V. of the Ti/Zr and sand/silt ratios. The Z.T.R. and C.P.A. indices assessed soil maturity and weathering rates. As a trial, these indices and other soil characteristics were connected with Rho by using statistical analysis to determine soil homogeneity and origin using the geophysical technique. The relationships between Rho and soil parameters at the study site show that, geophysical approaches may reliably predict and record soil property variations. Rho was shown to be strongly correlated with salic horizon (r=-0.91) causing a root limitation, lithic bedrock (r=0.92), porosity (r=0.89), clay (r=-0.79), sand (r=0.62), bulk density (B.D.), available water-holding capacity (A.W.H.C.), Z.T.R. (r=-0.78), C.P.A. (r=-0.74), and uniformity value (r=0.87). Standard regression curves were performed using Rho spatial trends in these characteristics. Results indicate that, apparent soil electrical resistivity measurements can accurately estimate soil origin and uniformity.

Key words: Apparent resistivity; Pedology, Soil uniformity, Genesis, Geophysical analysis.

INTRODUCTION

The soil's parent material is the factor that most decisively determines the soil's physicochemical, geochemical, and mineralogical properties and its uniformity within its pedon and origin (Hu *et al*., 2023). It is possible to evaluate the parent material, and its influence on soil should be researched to identify whether the parent material of each horizon is

*Corresponding author: dr.elwan@drc.gov.eg

uniform across the profile (Wang and Zhu, 2020). According to Wilson (2019), the various horizons or layers that make up a soil pedon often have distinct soil horizonation and features since they are derived from parent materials with distinct lithologies. When the homogeneity of the parent material is identified, the change in soil properties for different horizons in the profile can be attributed to either pedogenesis or geogenesis (Heidari *et al.,* 2022). Therefore, an accurate assessment of the vertical changes in soil pedon and parent materials has become an essential study method for soil pedogenesis and various types of soils (Schaetzl and Anderson, 2005; Wang and Zhu, 2020). The reason is that soil pedon and parent materials vary during a soil's vertical profile over time.

The grounding system design relies on soil resistivity, which measures the soil's ability to transmit or resist electric current and determines earth resistance (Tung and Lim, 2017). Improper soil resistivity analysis can lead to incorrect grounding system design. Soil resistivity must be minimized to design an effective grounding system for agriculture (Ya'acob *et al.,* 2023). When utilized for entire landscapes, typical soil survey methods for estimating horizon thickness within the soil pedon based on observations at soil pits or auger holes have methodological and cost limits (Wang and Zhu, 2020). These approaches are time-consuming, costly, and harmful, posing a hazard to soil resources (Ya'acob *et al.,* 2023). Since only point observations are available, mapping soil parameters of broad areas can be costly due to the need for numerous data points. Heidari *et al.* (2022) suggest geophysical approaches as an alternative to typical soil sampling methods. These methods are essential because soil qualities are intimately linked to geo-electrical properties. Research has shown a strong association between apparent electrical resistivity (ρ) and soil parameters such as clay content, water content, salt or nutrient content, and depth (Hu *et al.,* 2023).

Most published research focuses on geophysical mapping for soil property appraisal (Ya'acob *et al.,* 2023). While geophysics is commonly recognized, soil Rho or EC_e spatial changes are sometimes misinterpreted (Edouard *et al.,* 2023). Geophysical approaches for soil mapping capture the soil property's fluctuation and its impact on other properties (Lee *et al.,* 2023). To construct a successful geophysical survey for mapping soil features, it is essential to understand the correlations between Rho and soil parameters and deliver accurate data with little expense and labor (Zhu *et al.,* 2020). Limited research uses geophysical sensors to map soil variables with complicated relationships, such as Rho and multiple properties.

This study aimed to assess soil uniformity and genesis using pedological measurements and to assess correlations between Rho (ρ) in geophysical and pedological measurements of selected soil properties to enhance soil pattern mapping. This knowledge is crucial for determining soil mapping tactics and implementing geophysical technologies effectively. The research investigation took place in Wadi El-Madamude, east Luxor, Egypt, where the soil is vital for "life in this region". Using traditional soil survey methodologies to map several sites accurately can be costly. Testing alternate approaches, such as geophysical equipment, is necessary for mapping soil parameters in broad areas.

MATERIALS AND METHODS

Description of the Study Site

The study area for Wadi El-Madamude has a total area of 630.3 km^2. In the southeastern part of the Luxor governorate, it may be found between the latitudes and longitudes of 32° 30' and 33° 3' East, as well as 25° 23' and 25° 57' North (Fig., 1). This Wadi is controlled by two dams, as illustrated in Fig., 1. The Wadi El-Madamude has 8 main tributaries, they are from upstream to downstream, Wadi El-Kharit (18.6 km length), Wadi S.W. El-Madmude (16.9 km), Wadi S. El-Madmude (15.8 km), Wadi Abu-Garbasha (18.9 km), Wadi El-Rukhamyia (15 km), Wadi El-Bossat (12.6 km), Wadi El-Malah (13.9 km), and Wadi Banat Birri (12.3 km) at downstream (Table, 1 and Fig., 2a). Wadi El-Madamude has a gradient range of elevations varied from 75 m to 501 m from upstream to downstream (Table, 1 and Fig., 2b). The investigated area lies between a highly dissected

structurally controlled plateau in the East and the River Nile in the West. The eastern structural plateau is dissected by drainage basins that debouch towards the Nile (Fig., 2a) (El Shamy *et al.*, 2013). Each Wadi has a separate outlet to the Nile River. El-Madamude basin can receive flash floods (El Shamy *et al*., 2013).

Fig. (2b) shows the DEM of the Wadi El-Madamude study area (El Shamy *et al.*, 2013). Various geomorphologic units were found in the investigated Wadi. Old Nile terraces and Bajada plain are lowlands, while the Wadi El-Madamude midland, hydrographic system, and structural plateau are uplands. The old alluvial plain borders the young one. The mixture of sand and gravel forms terraces that rise to 25 m above the floodplain level. Incised dry streams of the drainage system continue from terraces to low areas of the young alluvial plain.

The Luxor area's eastern structural plateau is a distinct formation with its hydrographic system. The Nubian Sandstone rocks stretch south of Wadi Qena and Qena bend, forming the El Abbda plateau. Upper Cretaceous clastic and carbonate rocks topped Nubian sandstone. Rocks form the basis of the Luxor structural plateau. They are found beneath younger Paleocene, Eocene, and Pliocene strata, which are severely dissected by drainage channels (Fig., 3) (Ahmed, 2009). The eastern structural plateaus and dissected hills produce a conical watershed with dense drainage and a distinctive radial pattern. An inherent hydrographic system, originating from the structural plateau's higher extremities fragments the area and does not extend eastward. The hydrography of Wadi El-Madamude and its tributaries follows a typical radial pattern. Typically, these basins have deep and steep channels (El Shamy *et al.*, 2013).

Fig.(1): Wadi El-Madamude study area location.

Table (1): Description of Wadi El-Madamude mainstream and its main tributaries

Wadi El-Madamude tributaries	Length (km)	Elevation range (m; above sea level)
Upstreams		
Wadi El-Kharit	18.6	199-501
Wadi S.W. El-Madmude	16.9	298-426
Wadi S. El-Madmude	15.8	271-371
Wadi Abu-Garbasha	18.9	232-351
Midstream		
Wadi El-Rukhamyia	15.0	192-370
Wadi El-Bossat	12.6	148-273
Wadi El-Malah	13.9	132-333
Downstream		
Wadi Banat Birri	12.3	109-228
Wadi El-Madamude mainstream	**47.3**	**75-501**

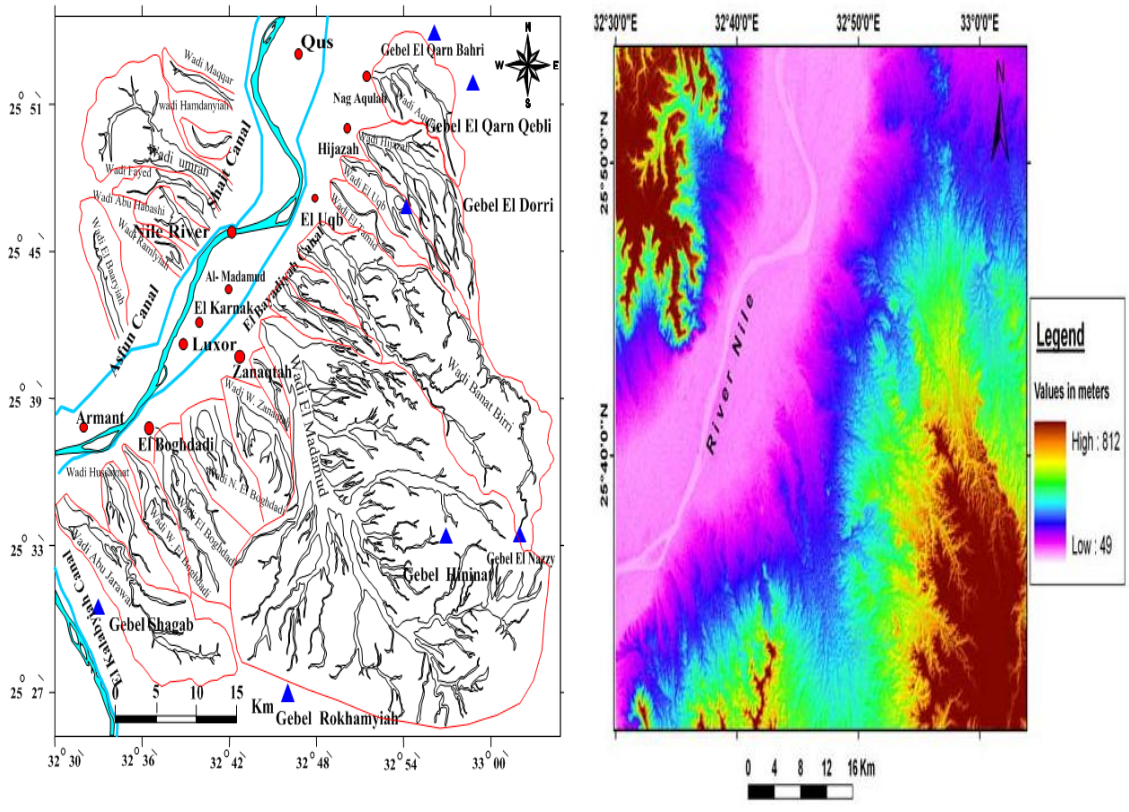

a) Hydrograpghic system **b) Digital elevation model (DEM)**

Fig. (2): Hydrograpghic system and DEM of Wadi El-Madamude basin (El Shamy *et al.*, 2013).

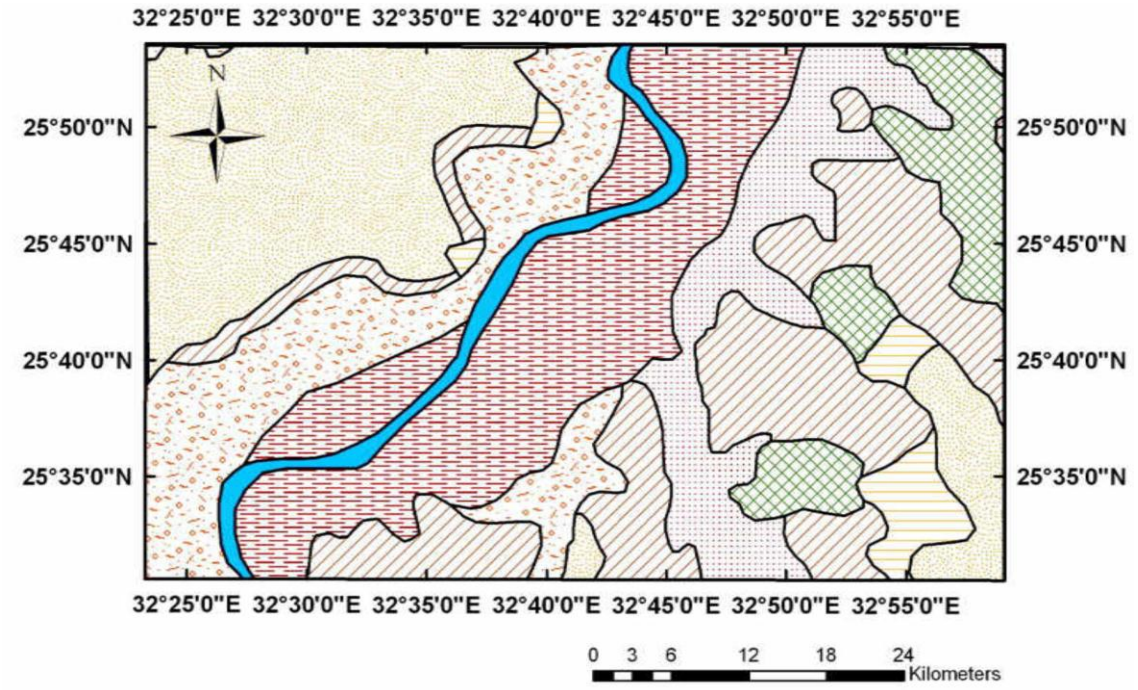

Fig. (3): Surface geological formations on lands of the Wadi El-Madamude study area (compiled from Ahmed, 2009).

According to the Egyptian Meteorological Authority (2022), Wadi El-Madamude's climate is desert-arid and changes yearly. The highest air temperature in July is 49.9°C, while the lowest is 22.7°C in January. Between May and December, the average monthly R.H. ranged between 25-55%. October had the highest average wind speed at 5.9 km/h, while April had the lowest at 9.3 km/h. Wadi El-Madamude experiences erratic, potentially negligible yearly precipitation (Ahmed and Fogg, 2014). Wadi El-Madamude morphometric analysis indicates a high flash flooding hazard degree 5, with 592 million cubic meters of water flow anticipated downstream to Bajada Plain (El Shamy *et al.,* 2013). Both surface and groundwater from the Nile were identified as irrigation supplies for the research location. Ahmed (2009) and Salman *et al.* (2019) identified two groundwater aquifers in Wadi El-Madamude: the shallow Quaternary Aquifer and the deeper Plio-Pleistocene Aquifer (Fig., 4; RIGW, 1997; Ahmed, 2009).

Sampling Scheme and Laboratory Methods

Initially, a field study survey using the pedon grid system and a hand auger was conducted to define the soil map based on the I.U.S.S. Working Group W.R.B. (2022). Around the pits, exploratory auger holes were dug to confirm the continuity of the soil layers/horizons. A hand auger was utilized to bring the most profound depth necessary to accurately describe the soil and obtain the required depth of soil pedons. Subsequently, four pedons were chosen to represent each type of soil and dispersed across the Wadi El-Madamude's catena, following the environmental gradient (76–501 m) from the southern East at the upslope to the northern West at the downslope (Fig., 5). Because understanding the unique soil matrix is crucial for accurate interpretation of physiochemical, geochemical, mineralogical, and geophysical results, a thorough characterization of the soil's characteristics was conducted to determine the relationship between the soil's features and its electrical resistivity values. The walls of every

soil pedon pit were thoroughly cleaned, and soil morphological descriptions were made *in situ* (color, structure, horizon boundaries, consistency, nodules, pedogenic features) following FAO (2006), Schoeneberger *et al*. (2012), Soil Science Division Staff (2017). According to I.U.S.S. Working Group W.R.B. (2022), the soils in the Wadi El-Madamude research area were divided into four reference soil groups (RSGs): Solonchaks, Regosols, Calcisols, and Leptosols. Soil horizons and layers designation was made following the master and suffix given by U.S.D.A. Soil Taxonomy of Soil Survey Staff (2022).

The representative pedons were chosen and examined based on soil types and the presence of soil-dominant features. Pedon 1 (P1) was selected to represent Leptosols and was situated in the upslope of Wadi El-Madamude before the dam building. In contrast, Pedon 2 (P2), symbolizing Regosols, was located near the dam at a midslope position. Furthermore, P3 and P4 were chosen downstream to indicate two different soil types: Calcisols and Solonchaks. Dam 2 is fronted by Pedon 3 (P3), and Pedon 4 (P4) is situated behind the dams and serves as a significant trap for all sediments transported from the upper regions.

The collected soil samples of each soil type were put in plastic bags, carried to the laboratory, and sieved with a 2-mm screen to remove roots, leaves, and other coarse fragments to prepare the soil samples for different studies. For laboratory investigations, a disturbed sample representative of each layer or horizon was gathered, and undisturbed samples of each layer were collected in metal rings (100 cm^3) for bulk density study.

Samples of air-dried soil were crushed and sieved to <2 mm. Laboratory analysis was conducted on the remaining fine-earth component. The pipette method for mechanical analysis was used to measure the particle size distribution of sand and clay (Sheldrick and Wang, 1993). Sand fractions were identified using dry sieving (Burt and Soil Survey Staff, 2014).

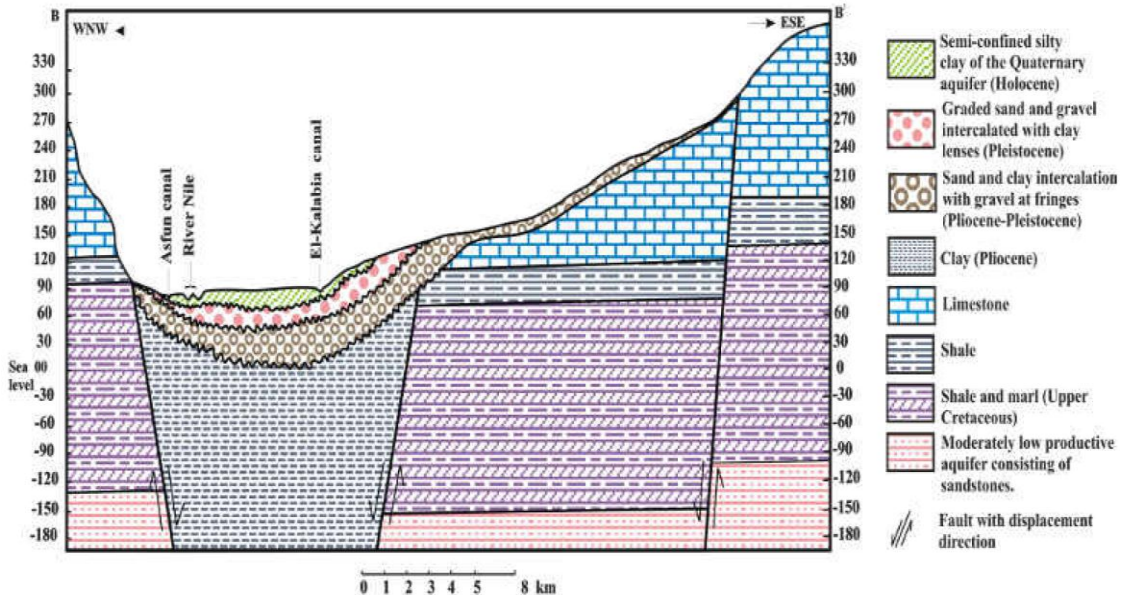

Fig. (4): Hydrostratigraphic section representing the Wadi El-Madamude study area (after RIGW, 1997; Ahmed, 2009).

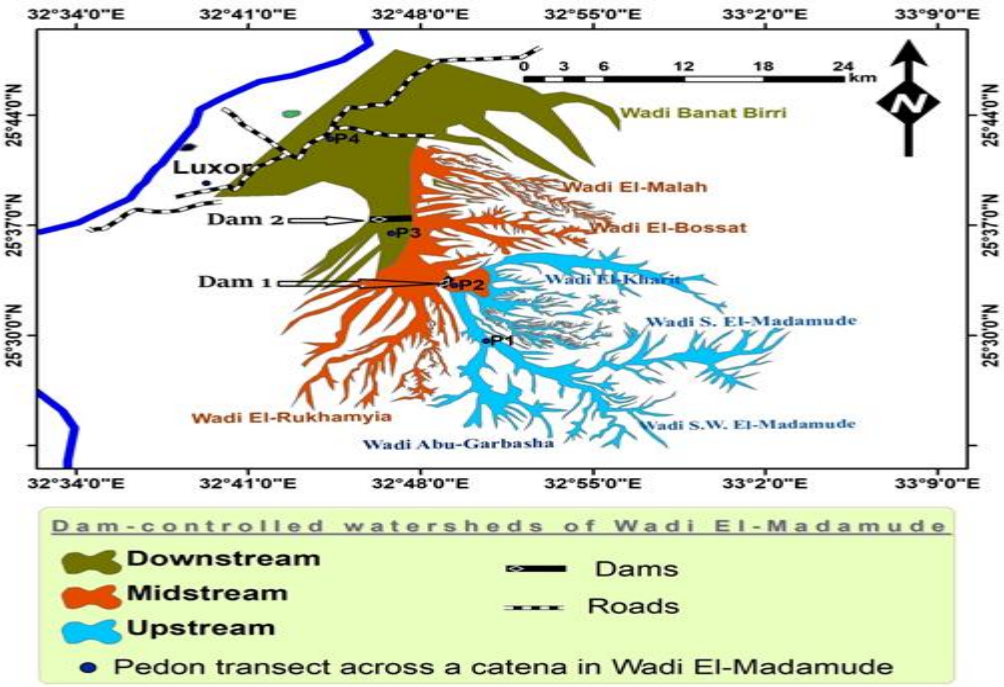

Fig. (5): Wadi El-Madamude landscapes and pedon transect across its toposequence.

Soil pH, EC_e, A.W.H.C., Calcium carbonate ($CaCO_3$), organic carbon (O.C.), and gypsum were measured per the standard soil analysis procedures adopted by Mani *et al*. (2007) and Burt and Soil Survey Staff (2014). The core sampling method was utilized for bulk density measurement (Lu, 2000; Grossman and Reinsch, 2002). The electric resistivity of the obtained soil samples was measured in the laboratory with a resistivity Ohm.m meter to determine the spatial distribution of the soil's resistivity. It was accomplished by measuring the electric resistivity. For a more accurate interpretation of the geophysical data, the soil data were incorporated into the analysis of the geophysical results. Additionally, a comparison of the geophysical study to the various layers and horizons of soil was performed.

Uniformity Index and Ratios Calculation

The uniformity value (U.V.) index is an effective tool for lithologic discontinuity detection. Lithologic discontinuities (L.D.s) exist when the parent material is not uniform (Schaetzl and Anderson, 2005). The uniformity value index (U.V.) of Cremeens and Mokma (1986) was employed to analyze soil particle size differences (silt and sand) (Formula 1).

$$U.V. = \left(\frac{\frac{(A+B)}{(X-B)} \text{ in overlaying horizon/layer}}{\frac{(A+B)}{(X-B)} \text{ in adjacent horizon/layer}} \right) - 1 \qquad (1)$$

Where U.V. indicates the uniformity value index of Cremeens and Mokma (1986), it demonstrates that horizons or layers in a pedon are likely generated from identical parent materials near zero, with A representing silt, B representing very fine sand, and X representing the entire sand component. Over 0.60 denotes lithologic discontinuity (L.D.) and nonuniformity in parent material (Schaetzl and Anderson, 2005).

The coefficient of variation (C.V.) of the Ti/Zr ratio and clay-free sand slit ratio were used to examine soil homogeneity based on the stable geochemical elements Ti and Zr. A C.V. of less than 22% for Ti/Zr suggests homogenous parent material. A sand slit ratio C.V. below 25% indicates homogeneous soil (Hu *et al*., 2023).

Microscopic Methods

Soil samples were sieved to 63-250 µm to identify heavy (>2.89 g/cm^3) and light minerals (<2.89 g/cm^3). A polarizing microscope was used to analyze the heavy minerals (Razum *et al.*, 2023). Sand fractionation based on the modified Wentworth size scheme by Walter *et al.* (1978) was used to determine the required fraction. An extra break at 63-µm was introduced to identify U.S.D.A. textural groups. The 63-250 µm fraction was selected for mineral analysis as it represents all mineral species proportionally. Heavy minerals in soil samples were prepared and separated using standard techniques, as revealed by Mange and Maurer (1992) and Mange and Wright (2007). Samples were treated with 30% hydrogen peroxide to remove organic matter. Decalcification was achieved with 20% hydrochloric acid. Bromoform ($CHBr_3$) extracted heavy minerals from this fraction at 2.85-2.88 g cm^{-3} density. Heavy minerals on glass slides were identified as Canada balsam using polarizing microscopes, with media reporting percentages. Each sample's percentage of non-opaque minerals was calculated from the total grains counted.

Provenance-sensitive heavy mineral ratios determine the parent rock of sediments. Examples include the Garnet-Zircon index (G.Z.i.) and the Rutile-Zircon index (R.Z.i.). The Tourmaline-Rutile index (Z.T.R.) was used to evaluate sediment maturity. Morton and Hallsworth (1994) developed the indices of G.Z.i. and R.Z.i. as reliable provenance indicators. Compared to Hubert (1962), the Z.T.R. index reveals the maturity of heavy mineral assemblages in sediments. GZi ratio (Equation 2) represents the percentage of garnet to total garnet + zircon. Although stable, garnets are heavy minerals. It is primarily found in metamorphic rocks but also magmatic rocks.

$$\text{G.Z.i.} = \left[\frac{\text{Garnet}}{\text{Garnet}+\text{Zircon}}\right] \times 100 \qquad (2)$$

In Equation 3, R.Z.i. is the percentage ratio of rutile to total rutile and zircon (Mange and Maurer, 1992). Rutile forms in metamorphic rocks, while zircon forms in plutonic rocks (Mange and Wright, 2007).

$$\text{R.Z.i.} \left[\frac{\text{Rutile}}{(\text{Rutile}+\text{Zircon})}\right] \times 100 \qquad (3)$$

Moreover, the Z.T.R. maturity index represents the fraction of non-opaque heavy minerals containing zircon, tourmaline, and rutile (Equation 4). The three minerals exhibit strong mechanical and chemical resistance to wear and strain. Improving sediment maturity leads to the breakdown of less stable minerals. Most resistant minerals remain stable and increase in relative abundance to sediment counterparts.

$$\text{ZTR} = \left[\frac{(\text{Zircon} + \text{Tourmaline} + \text{Rutile})}{(\Sigma \text{non} - \text{opaques})}\right] \times 100 \qquad (4)$$

The samples' mineralogical maturity was determined using the Z.T.R. index. The index value of 75% suggests immature to sub-mature sediments, while a Z.T.R. index of >75% shows mineralogically matured sediments, according to Hubert (1962).

Geochemical Analysis and Indices

The geochemical element oxides of Al_2O_3, SiO_2, Fe_2O_3, MgO, CaO, Na_2O, and K_2O were analyzed in the soil samples to study chemical weathering using an X-ray fluorescence spectrometer. The main assumption in creating chemical weathering indices is that the degree of weathering exclusively controls element behavior. According to Düzgören-Aydin *et al.* (2002), as weathering intensity increases, immobile oxides like Al_2O_3 and Fe_2O_3 remain constant, whereas mobile oxides like SiO_2, Na_2O, K_2O, CaO, and MgO decrease. The Na-type of the C.P.A. index was used to assess weathering (Buggle *et al.*, 2011). Ca-free C.P.A. is calculated using Equation 5. The presence of Na and Al in sediments indicates feldspar weathering, particularly plagioclase.

$$\text{C.P.A .}=[(Al_2O_3)/(Al_2O_3 + Na_2O)] \times 100 \qquad (5)$$

C.P.A. with higher values indicates more extensive chemical weathering. Nesbitt and Young (1982) found that C.P.A. values <55% imply physical weathering, while >55% indicates chemical weathering to varying degrees. SA and SAF ratios were calculated as follows: SA = (SiO_2/Al_2O_3) and SAF = [$SiO_2/(Al_2O_3 + Fe_2O_3)$] (Hu *et al.*, 2023).

Statistical Analyses

All of the required statistical analyses (such as the mean and standard deviation) were carried out with the help of the Statistical Package for the Social Sciences (SPSS) software (IBM® SPSS® Statistics). These analyses were then applied to the measured soil properties and Rho. The correlation coefficient, also known as Pearson's r, between the features of the soil on one side and the numerous soil properties (morphological, physiochemical, geochemical, and mineralogical) found vertically inside the studied pedons was used to assess the relationship between electrical resistivity and the different types of soil properties. Under the instructions provided by Rangaswamy (1995), the significance tests of the correlation coefficient and the regression analysis for the soil data were carried out. Based on the mean and standard deviation, the coefficients of variation (C.V.) of the titanium to zirconium ratio (Ti/Zr) and the C.V. of the sand/silt ratio were statistically determined for each of the two neighboring horizons/layers inside the soil pedon in the RSG (Hu *et al.,* 2023). These ratios were found to be statistically significant.

RESULTS AND DISCUSSION

Field Morphological, Physical, and Chemical Features

Tables (2) and (3) display all representative pedons' soil morphology, physical, chemical, and uniformity indices. All investigated pedons differ vertically in shape and texture across distinct layer sequences. All pedons tended for soil depth to rise with decreasing height. The deepest pedons were found at the lowest points of Wadi El-Madamude (P3 and P4). In contrast, upstream pedons absorbed more colluvial material and were shallower (P1). Different dams caught sediments from pedons 2 and 3, indicating intermediate (95 cm) to deep (145 cm) depth in P2. Pedon 3 at the dam-controlled watershed shares morphology and regolith depth with P4 downstream. Effective regolith depth ranges from 145 cm to 205 cm. Low-horizon redox concentrations in pedons were observed as oxidized iron (Fe^{+3}) masses in the matrix near depletions.

Soil texture in Wadi El-Madamude ranges from coarse sand on upslopes to loamy sand on midslopes to sandy clay loam and clay on the downslope. Upstream sand concentration was higher than downslope, ranging from 84.36 to 91.03% upstream and 23.30% to 74.95% downstream. Clay content was lower in upstream soils (4.59-5.5.66%) than that in downstream soils (7.05-41.05%), Table (2). The maximum clay content was found in the Btkz horizon of P4. Pedons of upslope in streams have the most extensive sand content, likely due to the coarse sedimentary material used to build upper Wadi El-Madamude deposits. P3 at downstream soils were Quaternary alluvial coarse sandy loam to sandy clay loam in a deep regolith (145 cm). P4 was found to be a very deep (205 cm) sandy-clay loam to clay with Ap horizon coverage at the downstream landscape site.

Parent material and slope determine gypsum and lime content. The gypsum content was 0.4-3.6% in upstream and less than 1% in midstream and downstream P3. Lower downstream areas have higher $CaCO_3$ values (8.6% to 25.4%). Calcareous sediment (1.3-1.9%) was only found in upstream pedons. Calcareous nature significantly affects midstream pedons compared to other slope positions. Table (2) indicates that downslope pedons are highly pedogenic because of high concentrations of secondary lime and iron. In downstream soils, secondary carbonate, and salt accumulation create calcic and salic layers in P3 and P4, respectively. The soils were classified as Calcisols for P3 and Solonchaks for P4 by I.U.S.S. Working Group W.R.B. (2022). Upstream soils were Leptosols, while midstream soils were Regosols (Table 2). Genetic horizon limits indicate dominant processes for soil formation, while layer borders indicate historical geogenic processes (FAO, 2006). The C layer borders in studied pedons differ in shape and slope position. Most pedons studied had abrupt, smooth borders (Table 2). Field evidence for L.D. includes pedons with smooth to broken and abrupt to diffuse boundaries (Schaetzl and Anderson, 2005; Burt and Soil Survey Staff, 2014). Upstream soils with the same parent

Table (2): Some morphological, physical characteristics, and reference soil groups across a toposequence of in Wadi El-Madamude

Pedon location	Horizon suffix	Horizon thickness (cm)	Root-restrictive and diagnostic horizon	Gravel (%)	Sand (%)	Clay (%)	C.V. of Sand/Silt ratio	U.V.	Porosity	R.S.Gs. as per I.U.S.S. Working Group W.R.B. (2022)
Upstream (P1)	C	0–17		39.6±2.87	84.36±3.65	4.59±1.12	0.36	0.17	High	**Leptosols**
	Cr	17–45		41.1±2.96	91.03±4.15	5.66±1.65	--	--		
	R	45+	Lithic bedrock	--	--	--	--	--		
Midstream (P2)	C	0–10		12.00±0.68	89.05±3.50	4.41±0.32	16.85	0.36	Medium	**Regosols**
	Ck	10–33	Fragipan	35.3±0.29	85.84±3.47	6.01±0.56	29.37	0.76		
	2Cm	33–70	Cemented layer	16.4±0.86	86.95±3.48	6.70±0.59	30.15	0.69		
	Cr	70–95		14.3±0.75	87.39±3.49	3.46±0.12	--	--		
Downstream (P3)	Ap	0–25		2.65±0.03	70.71±3.45	8.69±0.74	9.42	0.41	Low	**Calcisols**
	Bk	25–65	Calcic horizon	0.25±0.01	48.07±2.86	26.84±1.5	27.35	0.81		
	2Ck1	65–105		1.36±0.03	63.60±3.39	7.05±0.69	13.36	0.19		
	2Ck2	105-145		2.65±0.07	74.95±3.48	9.35±0.81	--	--		
Downstream (P4)	Ap	0–15		3.25±0.65	52.49±3.23	21.06±1.3	5.47	0.32	Very low	**Solonchaks**
	Bw	15–45		1.36±0.09	43.75±2.71	29.35±1.6	7.59	0.49		
	Btkz	45–70	Salic horizon	14.25±0.84	28.80±2.01	41.05±2.9	12.46	0.51		
	Btkm	70–115		10.36±0.96	27.02±1.98	32.68±2.3	15.27	0.09		
	Btm	115–155		9.65±0.19	50.35±3.15	22.01±1.2	17.41	0.51		
	Btg	155-205		3.65±0.07	23.30±1.05	21.69±1.1	--	--		
	W	205+	--	--	--	--	--	--		

Explanations: Horizon master and suffix designations were made based on Soil Survey Staff (2022). U.V. (Uniformity value): Each soil property's mean and standard deviation were statistically analyzed and calculated for each horizon/layer in the reference soil group (RSG). C.V. of sand/silt ratio (coefficient of variation of the sand to silt ratio) was statistically determined for each of two adjacent horizons/layers within the soil pedon in the RSG based on the mean and standard deviation.

Table (3): Physiochemical and electrical resistivity characteristics of studied pedons on a catena of Wadi El-Madamude

Pedon location & I.D.	Horizon suffix	B.D. ($g\ cm^{-3}$)	A.W.H.C. (%)	pH	EC_e (dS/m)	$CaCO_3$ (%)	Gypsum (%)	O.C. (%)	E.R. (Ω·m)
Upstream (Leptosols) P1	C	1.54±0.06	8.5±0.65	8.1±0.79	0.3±0.06	1.3±0.04	0.4±0.05	0.11±0.02	70129.3±32.5
	Cr	1.76±0.09	4.9±0.04	7.6±0.63	0.1±0.03	1.9±0.06	3.6±0.11	0.02±0.01	86475.6±45.9
	R	--	--	--	--	--	--	--	98120.5±12.03
Midstream (Regosols) P2	C	1.65±0.08	5.5±0.09	7.8±0.68	3.7±0.62	5.3±0.45	1.1±0.98	0.19±0.02	13546.1±11.03
	Ck	1.57±0.07	10.0±0.92	8.4±0.87	3.5±0.57	13.4±1.01	0.5±0.36	0.13±0.01	38634.2±15.36
	2Cm	1.59±0.04	9.4±0.82	8.0±0.74	4.8±0.66	6.6±0.51	0.6±0.05	0.01±0.04	41864.1±19.32
	Cr	1.61±0.05	4.8±0.96	7.9±0.81	3.2±0.54	5.2±0.43	0.1±0.03	0.04±0.01	59147.5±14.05
Downstream (Calcisols) P3	Ap	1.19±0.36	16.4±0.94	7.9±0.71	4.3±0.36	13.4±1.46	0.1±0.03	0.39±0.04	7126.3±6.32
	Bk	1.26±0.44	15.7±0.74	8.2±0.74	2.9±0.19	10.3±0.99	0.5±0.06	0.27±0.03	11264.9±2.65
	2Ck1	1.32±0.47	11.8±0.89	8.6±0.79	3.6±0.24	26.5±1.97	0.4±0.5	0.13±0.02	17258.4±14.02
	2Ck2	1.33±0.47	12.9±0.92	8.3±0.76	5.8±0.43	19.9±1.05	0.9±0.6	0.07±0.01	21357.2±13.61
Downstream (Solonchaks) P4	Ap	1.10±0.38	17.80±0.89	8.3±0.81	12.3±1.01	11.2±1.02	1.3±0.04	0.45±0.03	73.2±1.02
	Bw	1.27±0.55	13.50±0.85	8.7±0.84	8.1±0.78	15.3±1.25	2.4±0.09	0.31±0.02	67.9±3.15
	Btkz	1.53±0.98	14.20±0.66	9.1±0.89	15.2±1.23	25.4±1.98	0.9±0.01	0.37±0.03	53.6±1.89
	Btkm	1.69±0.79	15.30±0.76	8.9±0.88	9.6±0.89	14.7±1.53	1.1±0.07	0.11±0.02	64.1±4.16
	Btm	1.43±0.35	15.60±0.79	8.4±0.86	5.9±0.51	8.6±0.65	3.9±0.36	0.20±0.01	79.3±5.03
	Btg	1.39±0.28	16.40±0.83	7.8±0.69	6.8±0.56	10.1±0.98	2.7±0.04	0.12±0.01	55.1±2.69
	W								

Explanations: B.D. (Bulk density; A.W.H.C. (Available water holding capacity); O.C. (organic carbon); Electrical resistivity (E.R.); (Ω·m; Ohm.m.). Each soil property's mean and standard deviation were statistically analyzed and calculated for each horizon/layer in the reference soil group (RSG).

material have smooth, dispersed boundaries. P2 and P3 exhibited broken boundaries between Ck-2Cm and BC-2Ck1, indicating different source materials and deposition methods on previous surfaces. P4's wavy and smooth boundaries suggest the same materials (Table, 2). Visual analysis of rock fragments showed significant vertical changes in P2 strata (C, Ck) without pedogenic processes. In contrast, downslope pedons include less than 15% coarse fragments (Table, 2). Two L.D.s were identified in P2 and P3 as different alluvium sources. Rock fragment abundance morphology showed discontinuities at 10-33cm (Ck) and 33-70 cm (2Cm) for midstream soils and 25-65 cm (Bk) and 2Ck1 at 65-105 cm for downstream P3. L.D.s were not identified in other pedons (P4) at downstream of Wadi El-Madamude.

L.D.s were confirmepd by the uniformity index (U.V.) and C.V. of the sand/silt ratio (Table, 2). The difference in U.V. sand and silt separations on a carbonate-free, clay-free basis matched the vertical distribution of rock fragments in the pedon (Table, 2). Most analyzed pedons with high U.V. levels showed a sudden shift in PSD, not due to pedogenesis. The pedons of P2 at midstream on midlands and P3 at downstream on Bajada Plain were identified as L.D.s. The U.V. differences between two adjacent layers of these soils were greater than 0.60. The C.V. of the sand/silt ratio varied from 0.36% at upper slopes to 30.15 % at midstream. The soils of these pedons are not uniform, as shown by greater values than 25% between Ck and 2Cm of P2 and Bk and 2Ck1 of P3 (Table, 2). A similar trend for the same pedons was seen in Ti/Zr C.V.

Soil Electrical Resistivity Characteristics

Data on soil electrical resistivity (Rho) are shown in Table (3) and are graphically distributed vertically with soil depth and depicted in Fig (6). In upstream soils, it had a range of 70129.3-98120.5 Ω·m and a standard error (S.E.) of 12.03-45.9 Ω·m (Table 2). In midstream soils, it ranged from 13546.1 to 59147.5 Ω·m; downstream soils decreased to 55.1 Ω·m. Lower soil electrical resistivity values (79.3-55.1 Ω·m) are seen in the horizons of P4 at downstream.

Light Minerals

Light minerals in Wadi El-Madamude are primarily quartz and feldspar (Table, 4). Quartz is an inherited main mineral in soil from parent materials. Due to its weathering resistance compared to feldspars, the amount of quartz in the soil increases with time as less resistant minerals dissolve and throughout landscape position from upslope to downslope. Quartz is a key variable in the soil of Wadi El-Madamude. It is the most abundant mineral in the examined soils, ranging from 94.68% to 99.79%. Quartz-rich soil in this region is primarily created from sandstone colluvium or aeolian or alluvial deposits. High quartz contents are seen in soil produced on alluvial sand downstream of Wadi El-Madamude.

Soil properties are influenced by moisture and temperature (Woodruff *et al.,* 2015), and flooding substantially impacts element and mineral distribution in Wadi El-Madamude. Weathering of feldspar in soil along the gradient of higher precipitation from the eastern plateau to the West downstream is a fundamental alteration in soil composition. In soil, feldspar minerals react by hydrolyzing and leaching towards kaolinite, releasing Ca, Na, or K cations into solution. Feldspar occurs in soil from metamorphic and sedimentary rocks, but weathering has eliminated it in the investigated Wadi soil from identical parent materials (Yang *et al.,* 2018). Woodruff *et al.* (2015) found that most feldspar in the moderately weathered downstream may have changed to Al-rich clay. Feldspar loss ranges from 5.32% upslope to 0.21 downslope in soil, manifested by mineralogical transformation to kaolinite and gibbsite (Yang *et al.,* 2018) and chemical leaching of major and trace elements (Woodruff *et al.,* 2015).

Heavy Mineral Assemblages

The heavy mineral assemblage in Wadi El-Madamude varies based on lithology and slope position (Table, 4). The heavy minerals percentage increased from 3.95 to 15.32% on the slope gradient of Wadi El-Madamude, with

Table (4). Mineral percentages and mineralogical indices of sediments across the Wadi El-Madamude study area

Pedon ID[€]	Light minerals (%)		H.M.[†]	Opqu[†]	Non-opaque minerals[§]								Mineralogical indices[¶]		
	Quartz	Feldspar			Oliv.	Horn.	Aug.	Epid.	Kyan	Tourm.	Zirc.	Ruti.	Others	G.Z.i.	RZi	Z.T.R.
P1 (Upstream)	94.68±1	5.32±0.2	3.95±0.2	63.29±4	0.15±0.01	10.24±1.1	2.04±0.3	1.14±0.01	0.14±0.03	10.32±0.1	3.02±0.04	1.02±0.1	8.64±1.1	25.2	25.2	39.12
	95.02±2	4.98±0.6	4.01±0.3	59.22±3	0.15±0.02	11.02±1.2	1.06±0.4	1.62±0.02	0.74±0.05	9.32±0.02	2.05±0.06	2.30±0.3	12.52±0.3	56.1	52.9	33.52
P2 (Midstream)	96.35±3	3.65±0.4	5.32±0.5	37.71±1	0.26±0.04	13.62±0.3	2.47±0.05	1.24±0.04	0.95±0.04	11.32±0.5	11.02±0.1	3.62±0.4	17.79±1.4	28.2	24.7	41.68
	95.88±4	4.12±0.5	6.02±0.4	34.74±2	0.14±0.03	14.05±0.8	3.16±0.03	1.62±0.05	0.62±0.02	10.32±0.3	14.02±0.3	4.02±0.5	17.31±0.7	18.2	22.3	43.46
	97.35±4	2.65±0.3	7.23±0.9	36.4±3	0.16±0.07	12.31±0.9	1.25±0.08	1.95±0.01	1.63±0.06	9.32±0.2	15.32±0.1	5.32±0.6	16.34±1.4	14.7	25.8	47.11
	96.99±6	3.01±0.1	6.32±0.3	39.53±4	0.19±0.03	14.05±0.3	2.18±0.01	1.45±0.02	0.14±0.03	7.32±0.3	13.02±0.5	4.32±1.1	17.8±1.3	19.5	24.9	40.78
P3 (Downstream)	95.99±3	4.01±0.5	8.32±1.1	26.93±2	0.15±0.04	9.16±0.08	3.04±0.02	2.04±0.01	2.30±0.02	13.05±0.4	16.34±0.3	7.26±0.5	19.73±2.3	20.9	30.8	50.16
	96.38±1	3.62±0.9	6.32±0.3	34.01±1	0.14±0.01	7.06±0.61	1.02±0.01	2.62±0.03	1.04±0.05	11.35±0.1	15.02±0.8	6.32±0.7	21.42±2.4	19.6	29.6	49.54
	96.79±2	3.21±0.7	7.32±0.8	20.19±2	0.36±0.02	6.35±0.31	2.51±0.04	3.12±0.05	2.13±0.06	16.32±0.5	15.32±0.9	7.32±1.3	26.38±0.9	32.0	32.3	48.82
	97.92±4	2.08±0.5	8.32±0.6	22.17±3	0.41±0.03	5.32±0.01	3.05±0.09	2.04±0.01	1.08±0.03	15.02±0.6	14.32±1.1	7.26±0.7	29.33±4.1	27.1	33.6	47.03
P4 (Downstream)	98.05±5	1.95±0.7	9.12±0.5	27.58±2	0.17±0.01	1.05±0.03	0.15±0.01	2.01±0.01	0.36±0.01	16.32±1.4	18.32±1.6	21.3±2.9	12.74±0.5	8.3	53.8	77.24
	98.93±3	1.07±0.9	10.32±1	6.01±0.1	0.16±0.02	0.96±0.01	1.05±0.02	1.62±0.02	0.41±0.01	26.32±1.1	27.32±2.3	23.32±1.6	12.83±0.3	7.4	46.1	81.88
	98.99±2	1.01±0.3	15.32±2	4.73±0.9	0.24±0.07	1.35±0.05	2.15±0.04	1.04±0.01	1.32±0.01	19.32±0.2	23.04±2.9	33.25±1.3	13.56±0.7	18.5	59.1	79.36
	99.79±1	0.21±0.5	13.01±1	7.27±0.5	0.36±0.03	0.14±0.01	1.34±0.03	0.65±0.01	0.01±0.0	20.10±1.2	23.32±1.7	26.31±3.2	20.5±3.4	11.9	53.0	75.20
	99.02±4	0.98±0.2	10.24±2	3.19±0.2	0.24±0.05	0.2±0.01	2.04±0.11	3.15±0.03	1.11±0.01	27.35±2.3	25.42±1.2	23.01±2.1	14.29±1.3	11.3	47.5	78.28
	98.96±2	1.04±0.4	13.95±4	12.02±4	0.31±0.04	1.29±0.01	1.74±0.02	2.14±0.02	1.24±0.01	17.35±0.5	19.35±0.8	29.32±1.3	15.24±1.4	21.6	60.2	75.04

Explanations: [€]Pedon 1 is on upstream of the Wadi El-Madamude; Pedon 2 represents the midstream of the studied Wadi; Downstream of the Wadi was sampled by pedons 3 and 4.

[†] H.M. (heavy mineral concentration); [†]Opqu (opaques); [§]Oliv. (olivine), Horn. (hornblende), Aug. (augite), Epid (epidote), Kyan. (kyanite), Tourm. (tourmaline), Zirc. (zircon), Ruti. (rutile);

[¶] G.Z.i. (garnet-zircon index), R.Z.i. (rutile-zircon index), Z.T.R. (zircon-tourmaline-rutile index).

Table (5): Geochemical characteristics of sampled pedons on a catena of Wadi El-Madamude

Pedon location and soil type	Horizon thickness (cm)	SiO_2 (%)	Al_2O_3 (%)	Fe_2O_3 (%)	MgO (%)	CaO (%)	Na_2O (%)	K_2O (%)	C.V. of Ti/Zr ratio	Weathering indices†		
										C.P.A. (%)	S.A. ratio	S.A.F. ratio
Leptosols (Upstream)	R	82.32±6.3	5.04±	11.02±1.3	1.02±0.24	2.45±0.7	5.32±1.2	4.35±0.5	14.2	48.65	16.33	5.13
	Cr	81.02±7.1	4.58±	10.02±1.9	2.35±0.09	3.21±0.8	4.32±1.6	5.01±0.7	16.3	51.46	17.69	5.55
	R	Bedrock										
Regosols (Midstream)	C	71.32±5.3	5.84±0.8	13.03±1.9	0.36±0.04	4.26±0.5	4.05±0.9	3.62±1.6	20.1	59.05	12.21	3.78
	Ck	75.62±1.3	4.83±0.5	14.15±0.4	1.62±0.02	2.36±0.6	4.32±0.5	3.07±0.4	26.3	52.79	15.66	3.98
	2Cm	74.32±5.3	4.47±0.2	12.03±0.8	3.25±0.95	4.15±0.3	4.17±0.7	2.54±0.7	24.3	51.74	16.63	4.50
	Cr	71.09±8.1	3.15±0.4	14.20±1.6	4.32±0.71	6.32±0.4	4.26±0.3	5.98±0.9	--	42.51	22.57	4.10
Calcisols (Downstream)	Ap	64.32±2.7	5.25±0.6	10.25±2.3	1.32±0.25	10.36±0.1	3.65±0.4	3.01±0.5	11.2	58.99	12.25	4.15
	Bk	63.21±9.6	4.94±0.8	7.32±1.7	1.06±0.36	7.32±1.4	4.05±0.6	2.65±0.3	23.6	54.95	12.80	5.16
	2Ck1	69.32±3.6	5.11±0.3	8.12±0.9	2.32±0.24	13.25±2.6	3.45±0.8	2.98±0.7	28.3	59.70	13.57	5.24
	2Ck2	61.02±2.9	4.19±0.7	9.01±0.8	3.02±0.19	11.32±1.7	3.62±0.7	2.07±0.6	--	53.65	14.56	4.62
Solonchaks (Downstream)	Ap	59.62±1.7	14.12±1.6	6.32±0.7	3.14±0.08	9.41±0.9	1.98±0.4	3.12±0.01	21.3	87.70	4.22	2.92
	Bw	57.32±2.8	14.05±1.5	4.32±0.6	4.02±0.31	14.32±2.6	2.36±0.5	1.75±0.02	19.4	85.62	4.08	3.12
	Btkz	54.36±4.6	14.35±1.7	4.01±0.5	5.03±0.47	15.25±1.3	2.41±0.6	1.36±0.4	11.2	85.62	3.79	2.96
	Btkm	49.35±2.4	13.05±1.6	3.26±0.4	5.78±0.95	13.65±2.7	1.15±0.2	2.05±0.01	20.3	91.90	3.78	3.03
	Btm	54.32±3.9	13.12±2.1	5.45±0.3	4.51±0.14	7.32±0.9	1.32±0.5	1.99±0.03	18.4	90.86	4.14	2.93
	Btg	48.62±2.8	11.94±0.9	4.21±0.9	4.36±0.36	10.32±2.3	1.05±0.4	2.01±0.09	--	91.92	4.07	3.01
	W	Watertable level										

Explanations: † C.V. of Ti/Zr ratio (coefficient of variation of the titanium to zirconium ratio); C.P.A. (%)= $[(Al_2O_3)/(Al_2O_3 + Na_2O)] \times 100$; SA=$(SiO_2/ Al_2O_3)$; SAF=$[SiO_2/(Al_2O_3+ Fe_2O_3)]$

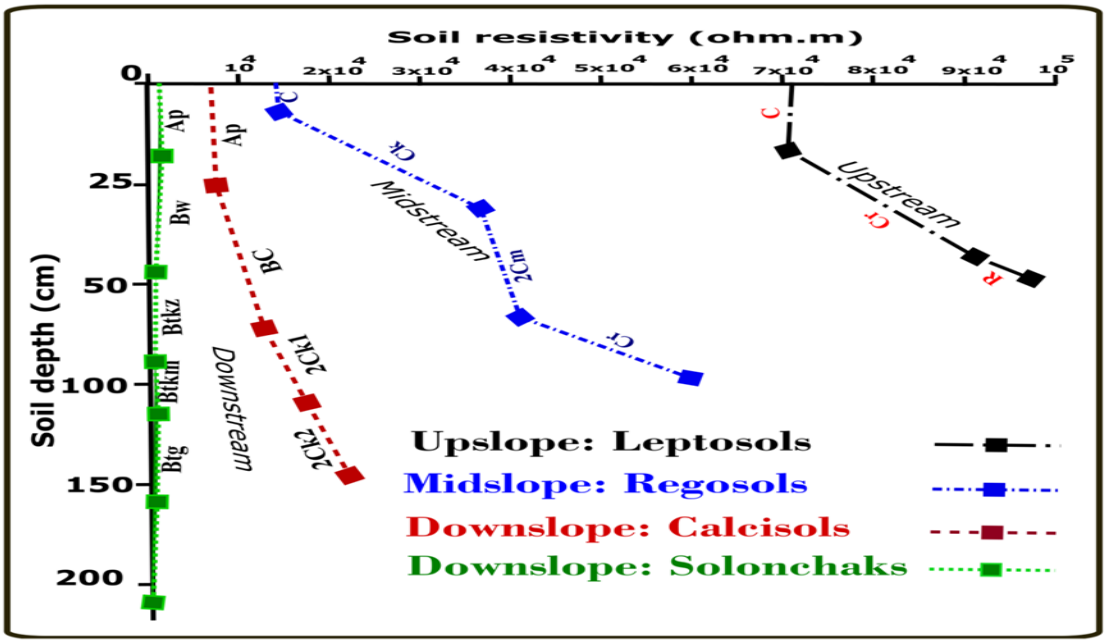

Fig. (6): A comparison of the soil electrical resistivity trends among pedons vertically with depth across the Wadi El-Madamude toposequence.

a clear transition from upper to lower slopes. At the dam1-controlled watershed, heavy mineral concentrations ranged from 3.95% in upslope to 4.23% in midslope, increasing with decreasing elevation. Heavy mineral concentrations were highest (6.32-15.32%) in the plain of Wadi El-Madamude. Deposition of stability-heavy minerals from upstream tributaries and adjacent lithology may explain the rising trend. The distribution of heavy minerals in Wadi sediments is linked to the lithology of the rocks investigated. The Wadi sediments, from higher rivers to downstream lowlands, contained heavy minerals such as tourmaline, rutile, zircon, zoisite, kyanite, epidote, augite, hornblende, olivine, and opaques. The heavy mineral assemblage ranged from ultrastable to highly unstable (Table, 4). Hornblende and augite decrease from upstream to downstream, whereas epidote, zircon, rutile, and tourmaline increase in the downslope of Wadi El-Madamude.

Opaques (3.19-63.29%), hornblende (0.14-14.05%), zircon (2.05-27.32%), and tourmaline (7.32-27.35%) were the main heavy minerals in soils of Wadi El-Madamude. Upstream sediments consist of opaques (59.22-63.29%), kyanite (0.14-0.74%), zircon (2.05-3.22%), epidote (1.14-1.62%), tourmaline (9.32-10.32%), rutile (1.02-2.30%), zoisite (0.14-1.21%), hornblende (10.24-11.02%), and olivine (0.15%). In Wadi El-Madamude's downslope deposits, zircon (18.32-27.32%), tourmaline (16.32-27.35%), and rutile (21.3-33.25%) dominated the heavy mineral suite (Table, 4). The provenance GZi index ranged from 7.39 to 56.1% in the downslope, whereas the RZi index ranged from 22.28% to 60.2% in the deepest lowland soil layer. The maturity Z.T.R. index went from 33.52% upslope to 81.88% at downstream in the P4 subsurface horizon. Low Z.T.R. index values (<75%) indicate immature sediments at these sites due to geomorphic instability and fast erosion (Razum *et al.*, 2023). Table (4) shows that, sediments in downstream soils are mature (>75%). Minerals such as garnet, kyanite, zoisite, and staurolite suggest high-rank metamorphic rock, whereas biotite, hornblende, and monazite indicate acid igneous rock. Augite, olivine, and augite show basic igneous rock (Razum *et al.*, 2023). The non-opaque mineral assemblage comprises ultrastable (zircon, tourmaline, rutile), stable (garnet, staurolite, biotite, monazite), moderately stable (epidote, kyanite, zoisite), unstable (hornblende, augite), and highly unstable (olivine) minerals.

The low stability indices of G.Z.i. and R.Z.i. suggest the origin of the granitic and plutonic rock. The Wadi's parent rocks likely consist of limestones, sandstones, and alluvial deposits. Both diorite and ferruginous sandstone were the primary lithologies. Sandstones in the upper slopes are primarily responsible for sedimentation.

Additionally, sediments in deep soils beneath check dam 2 primarily comprise hornblende, monazite, tourmaline, zircon, and rutile. Due to the need for recycling ultrastable heavy minerals, unstable minerals like olivine are less prevalent in this area. The presence of staurolite, kyanite, and garnet indicates a metamorphic rock origin of greenschist to amphibolite. Wadi El-Madamude sediments are derived from limestone and high-grade metamorphic rocks. The lowland (P4) sediments were combined at the downstream landscape point. Fine soil along the Nile floodplain was covered by recently transported coarse materials from desert hydrographic basins, resulting in fine-textured soil. They originated from the Nile flood process of exquisite items. The soils have been enriched by recent coarse deposits from highland areas (e.g., midstream and upstream).

Geochemical Properties of Soils

Table (5) shows the geochemical properties of soils across Wadi El-Madamude. Generally, Si, Al, and Fe oxides dominated primary element oxides in sediments from all streams in Wadi El-Madamude. The soils analyzed contained substantial components such as Al_2O_3, SiO_2, and Fe_2O_3, ranging from 95.62-98.39% in upstream to 64.77-75.69% at upslope. The geochemical study revealed that the sediments of Wadi El-Madamude include 48.62-82.32% SiO_2, 3.15-14.35% Al_2O_3, 3.26-14.20% Fe_2O_3, 0.36-5.78% MgO, 2.36-15.25% CaO, 1.05-5.32% Na_2O, and 1.36-5.98% K_2O (Table, 5). SiO_2, Na_2O, and K_2O concentrations decreased in downstream weathered sediments relative to upstream, rising with weathering and distance from the source rock. This may be due to direct loss during feldspar breakdown. Unlike the usual trend, CaO content increased with a lowering slope and increasing weathering, likely due to secondary carbonates (Tables, 3 and 5). Research suggests that oxidation is crucial for iron-bearing minerals like biotite in Wadi El-Madamude. Soil concentrations of SiO_2 were substantially more significant on the upslope than on the downslope. The soils' increased SiO_2 concentration is due to the prevalence of quartz in the samples. However, Fe-containing minerals like hematite and goethite may explain the observed ferric oxide concentrations.

Particular oxide concentrations measure soil weathering. Weathering indices are routinely used to assess chemical changes in various materials (Darmody *et al.*, 2005). The indices are based on the ratio of mobile elements (e.g., SiO_2, CaO, MgO, Na_2O) to immobile (e.g., Al_2O_3 and Fe_2O_3) elements that should decrease with time during leaching. Table (5) displays weathering indices for all pedons and their horizons/layers. C.P.A. values ranged from 42.51 to 91.92%. The most significant values were found on the downslope, indicating chemical weathering. S.A. ratio ranged from 3.78 in P4 from downslope to 22.57 in P2 at midstream, while S.A.F. was 2.93 from downstream to 5.55 at upstream.

Using geochemical and weathering indices can enhance our understanding of soil origin and uniformity. Knowing how weathered a regolith is can be helpful (Schaetzl and Anderson, 2005). The degree of weathering often correlates with soil growth and mobility. Weathering is the slow transition of parent material into more stable minerals through morphological, physicochemical, and geochemical changes (Buggle *et al.*, 2011). Weathering can alter the element composition of a parent material. Chemical weathering indices assume that, the action of chemical components is solely determined by the degree of weathering. The earth alkali elements Ca, Na, Mg, and K are geochemically mobile. Yang *et al.* (2004) found that, Al, Fe, and Ti are less impacted by chemical leaching and focus on weathering products. These elements are classified as soluble cations based on their ionic potential. Solubility does not always imply mobility (Buggle *et al.*, 2011). Increasing radius leads to increased ion adsorption on clay minerals, reducing mobility. Earth alkali elements Ca and K, with reduced ionic radius, are found in weathering-prone silicate minerals such as plagioclase, pyroxene,

amphibole, and biotite (Nesbitt and Young, 1984). Redox conditions may regulate some element distribution. Employing the elements Fe and Mn in weathering experiments is not advised. According to Buggle *et al.* (2011), the C.P.A. index is based on the idea that, Na^+ is released and mobilized during weathering, while Al^{3+} is kept and forms secondary clay minerals and Al-oxides. The feldspar group is the primary host mineral group for Na and Al in unweathered protoliths. This group produces clay minerals and aluminous leftovers like kaolinite ($Al_2Si_2O_5(OH_4)$) or gibbsite ($Al(OH)_3$) after significant weathering.

Wadi El-Madamude sediments show more immobile components in downslope soil than upslope soil. In contrast, mobile element concentrations decrease, except for CaO, which increases in calcareous deposits as in the downslope. As weathering progresses, SiO_2 concentration declines, but Al_2O_3 content displays small reductions. In carbonate-rich parent materials of Wadi El-Madamude deposits, calcite and dolomite have a significant role in controlling Ca and Mg mobility. Using silicate Ca estimates in calcareous materials may skew weathering records due to carbonate dynamics interferences. This results in misleadingly low indices relative to C.P.A. (Table, 5) and underestimates weathering intensity. The contribution of carbonate Ca to measured CaO in calcareous material may lead to inaccurate results. The geochemistry of sediments in the dam-controlled Wadi El-Madamude watershed suggests chemical weathering in downslope due to water harvesting using check dams, compared to erosion-prone upslope without dams (Yang *et al.*, 2018). Rocks undergo physical weathering to reduce grain size without generating geochemical or mineralogical changes, with geochemical indices below 55% indicating no chemical weathering. Diagenetic effects from secondary carbonate or K-fixation (illitization) are not a concern, unlike Na-type indices (CaO and K_2O), Heidari *et al.*, (2022). These findings show chemical weathering limited to higher altitudes on the dam-controlled watershed of Wadi El-Madamude and lower elevations downstream. To prevent silicate weathering, use carbonate-free parent material when using such indices. The C.P.A. index is recommended for silicate weathering in calcareous sediments to avoid uncertainties in CaO determination due to secondary carbonates (Heidari *et al.*, 2022).

Relationship between Soil Characteristics and its Electrical Resistivity

The correlation matrix and regression analyses show that soil electrical resistivity (Rho; ρ) significantly correlated with different soil criteria and computed indices based on the mechanical composition of soil texture, mineralogical, and geochemical properties (Tables 6 and 7). Several soil variables, such as morphological, physical, chemical, geochemical, and mineralogical properties, in addition to the uniformity, weathering, and maturity indices, were used to validate the effectiveness of the electrical resistivity further to forecast the soil variables. Root-restrictive layers, porosity, clay, sand, gravel, EC_e, $CaCO_3$, gypsum, E.S.P., O.C., C.E.C., SiO_2, Al_2O_3, Fe_2O_3, Mgo, CaO, Na_2O, K_2O, Quartz, feldspars, opaques, hornblend, zircon, tourmaline, rutile, U.V., C.P.A., S.A., S.A.F., G.Z.i., R.Z.i., and Z.T.R. are some of these characteristics. Electrical resistivity (m) and all of these properties were correlated. Significant correlations existed among soil variables (Table, 6). Sand content in studied soils was negatively correlated with clay (r=-0.68), O.C. (r=-0.65), EC (r=-0.49), and C.E.C. (-0.39) and positively correlated with SiO_2 (r=0.91), Al_2O_3(r=47), and gypsum (r=0.35), Table (6). There was a high positive or negative correlation between clay and C.E.C. (r=0.84), A.W.H.C. (r=0.81), O.C. (r=0.76), Fe_2O_3 (r=0.72), EC (r=0.71), B.D. (r=0.62), and Al_2O_3 (r=-0.60). The bulk density has a positive connection with Fe_2O_3 (r = 0.73), gravel (r = 0.63), sand (r = 0.49), and SiO_2 (r = 0.47), and a negative correlation with clay (r = -0.62), O.C. (r = 0.72), and A.W.H.C. (r = -0.69) (Table, 6).

By employing the correlation coefficient (r) and regression analysis, the findings shown in Table (7) demonstrated that, the soil constituents had a strong relationship with the soil electrical resistivity (Ω·m). While the Rho was found to have a negative correlation with the amount of clay present (r = -0.79). It was found to correlate

Table (6): Pearson correlation coefficient between the traditionally analyzed soil attributes

Soil attribute	Sand (%)	Gravel (%)	Clay (%)	O.C. (%)	pH (%)	E.S.P. (%)	EC (%)	A.W.H.C. (%)	Gypsum (%)	$CaCO_3$ (%)	Fe_2O_3 (%)	Al_2O_3 (%)	SiO_2 (%)	C.E.C. (cmol/kg)	B.D. (g cm^{-3})
Sand (%)	1.00														
Gravel (%)	0.07^{NS}	1.00													
Clay (%)	-0.68^{**}	-0.24^{**}	1.00												
OC (%)	-0.65^{**}	0.39*	0.76^{**}	1.00											
pH (%)	-0.31^{*}	0.15^{NS}	0.51^{*}	-0.45^{*}	1.00										
ESP (%)	-0.42^{*}	0.11^{NS}	0.64^{*}	-0.30^{*}	0.79^{**}	1.00									
EC (%)	-0.49^{**}	-0.57	0.71^{*}	-0.51^{*}	-0.52^{*}	0.44^{*}	1.00								
AWHC (%)	-0.78^{**}	-0.43^{**}	0.81^{**}	0.91^{*}	-0.48^{*}	-0.42^{**}	-0.53^{*}	1.00							
Gypsum (%)	0.35^{**}	0.11^{NS}	0.62^{*}	-0.38^{**}	-0.37^{*}	0.39^{*}	0.68^{*}	0.33^{*}	1.00						
$CaCO_3$ (%)	0.15^{NS}	0.1^{NS}	0.32^{*}	-0.59^{**}	0.89^{**}	0.58^{**}	-0.35^{*}	0.55^{**}	0.43^{*}	1.00					
Fe_2O_3 (%)	0.18^{NS}	0.05^{NS}	0.32^{*}	-0.45^{**}	-0.43^{*}	0.35^{*}	0.16^{NS}	0.61^{*}	0.11^{NS}	0.20^{NS}	1.00				
Al_2O_3 (%)	0.47^{**}	0.24^{**}	-0.60^{**}	-0.44^{**}	-0.49	-0.24^{*}	0.17^{NS}	0.32^{*}	0.12^{NS}	0.10^{NS}	0.45^{*}	1.00			
SiO_2 (%)	0.91^{**}	0.51^{*}	-0.49^{**}	-0.63^{**}	-0.32^{*}	0.42^{*}	-0.43^{**}	0.71^{**}	0.33^{**}	0.13^{NS}	0.17^{NS}	0.43^{**}	1.00		
CEC (cmol/kg)	-0.39^{**}	-0.44^{*}	0.84^{**}	0.98^{**}	0.07^{NS}	0.11^{NS}	0.13^{NS}	0.55^{*}	0.34^{*}	-0.38^{*}	-0.47^{*}	0.41^{*}	-0.75^{*}	1.00	
B.D. (g cm^{-3})	0.49^{**}	0.63^{*}	-0.62^{*}	-0.72^{*}	0.22^{NS}	0.23^{NS}	0.08^{NS}	-0.69^{*}	-0.41^{*}	-0.47^{**}	0.73^{*}	0.42^{*}	0.47^{*}	-0.49*	1.00

**Significant at $p< 0.01$.

* Significant at $p< 0.05$.

Table (7): The correlation coefficient (Pearson's r) of several soil parameters with soil electrical resistivity at different significant levels.

Electrical resistivity, Rho (Ω·m)						
Estimated soil properties						
Root-restrictive layers vertically within soil pedon						
Abrupt textural change	**Cemented horizon**	**Fragipan**	**Salic**	**Petrocalcic**	**Lithic bedrock**	
0.51*	-0.75**	0.73**	-0.91**	-0.680*	0.92**	
Physical properties						
Porosity	**Clay (%)**	**Sand (%)**	**Gravel (%)**	**B.D.**	**A.W.H.C.**	
0.89*	-0.79**	0.62*	0.84**	0.91**	-0.87**	
Chemical properties						
pH	**EC_e**	**$CaCO_3$**	**Gypsum**	**E.S.P.**	**O.C.**	**C.E.C.**
0.49*	-0.88**	-0.70*	-0.54*	-0.65**	-0.73*	-0.55**
Geochemical characteristics						
SiO_2	**Al_2O_3**	**Fe_2O_3**	**MgO**	**CaO**	**Na_2O**	**K_2O**
0.61*	**-0.49***	**-0.72**	**0.20NS**	**0.12NS**	**0.48***	**0.09NS**
Mineralogical components						
Quartz	**Feldspars**	**Opaques**	**Hornblen**	**Zircon**	**Tourmalin**	**Rutile**
0.64*	**-0.74****	**0.67***	**-0.34***	**-0.65***	**-0.42****	**-0.34***
Uniformity, mineralogical, and weathering indices						
UV	**CPA**	**SA**	**SAF**	**GZi**	**RZi**	**ZTR**
0.87**	**-0.74****	**-0.56***	**-0.32***	**0.41***	**0.35****	**-0.78***

* (Significant at 5% level); ** (Significant at 1% level); N.S. (Not significant); B.D. (Bulk density); A.W.H.C. (Available water holding capacity); E.S.P. (Exchangeable sodium percentage), O.C. (Organic carbon); C.E.C. (Cation exchange capacity).

positively with the amount of sand and gravel present. Rho was found to have a positive association with fragipan and lithic bedrock. At the same time, the highest negative correlations were identified with the presence of cemented pan, salic, and petrocalcic horizons inside the soil pedon as morphological criteria. In terms of the correlation between physical properties with Rho, the highest positively significant correlations were observed for bulk density (r =0.91), and porosity (r =0.89), gravel (r =0.84), and sand (r = 0.62) and the negative correlation was found with clay (r = -0.79) and A.W.H.C. (r =-0.87). For chemical and geochemical parameters and Rho, the highest negative correlation was for ECe (r =-0.88), Fe_2O_3 (r=-0.72), O.C. (r =-0.73), $CaCO_3$ (r =-0.70), and), C.E.C. (r = -0.55)and Al_2O_3 (r=-0.49). In contrast, the lowest correlation was obtained for pH (r =0.49. Regarding the heavy and light minerals in soils, the correlation between the light and heavy minerals and Rho varies depending on the type of mineral. For example, quartz has a positive correlation (r=0.64), and feldspar has a negative correlation (r=-0.74). The correlations between the heavy minerals also vary; for example, rutile has a negative correlation (r = -0.34), whereas zircon has a negative correlation (r = -0.65), hornblende has a positive correlation (r=-0.31), and tourmaline has a negative correlation (r = -0.42) (Table, 7).

As presented in Figs. (7 to 13), soil electrical resistivity measurements in the laboratory have been used to develop predictive equations for the

more significant soil variables. The results generally concluded that, finer soil texture has an electrical charge than coarse-textured soils. Sand, silt, clay, and organic matter are the constituents of soils. Clay and organic matter particles have a net negative charge and function well as electrical connections. In the same way that a magnet's opposite poles attract one another, these negatively charged soil particles will draw in and retain positively charged particles.

In contrast to clay and O.C., the sand particles served as electrical impedance since they had low charges and were poor electrical conductors. As a result, there is a positive association between Rho and sand content and a negative correlation between clay particles and Rho. The electrical conductivity of the soil's constituents steadily decreases as soil porosity increases while the Rho increases. Thus, there is a strong positive association between soil porosity and Rho. Regarding the relationships between the computed indices and Rho, the UV, GZi, and RZi all show a positive correlation; however, the weathering and maturity indices have a negative connection. While there is a significant positive association between the U.V. index and Rho (r = 0.87), there is a significant negative correlation between the Z.T.R. index and Rho (r = -0.78) (Table, 7 and Fig., 13).

Based on the findings, it was deduced that, the low values of Rho reflected the very mature and weathered sediments and the highly pedogenetic processes that led to clay production. The higher values of Rho represent the poor genesis and development of soils with high gravel and sand contents in the sediments. These soils have high Rho values because the soils contain a lot of gravel and sand. Consequently, the Rho values of highland sediments are pretty high; high concentrations of sand, gravel, and colluvial elements characterize these sediments. While the midstream soils have a moderate range of Rho, the downstream soils have very low values of Rho, and these soils are characterized by having high levels of clay, A.W.H.C., calcic horizon(Bk) in P3, and salic (Btkz) in P4, and increased soil profile development with a sequence of Ap-Bw-Btkz-Btkm-Btm-Btg-W. The Btg has a very low Rho value (55.1 Ω·m) (Table, 3).

Figs. (7 through 16) show the regression curves that, were performed between the measured characteristics of the soil and the predicted electrical resistivity of the soil for all of the soil variables. Clay content (R^2 = 0.75; Fig., 7), sand (R^2 = 0.69; Fig., 8); soil porosity (R^2 = 0.85; Fig., 9); C.P.A. index (R^2 = 0.71; Fig., 11); uniformity value index (R^2 = 0.54; Fig., 12); and Z.T.R. maturity index (R^2 = 0.69; Fig., 13) were shown to have the strongest predictive models. According to the findings, most of the soil's electrical resistivity was significantly related to clay, the amount of iron oxide present, and the soil's organic carbon (O.C.) content, all of which could be precisely predicted. The trend of the silica constituent was the same as that of the sand content (Table, 7), which showed that the presence of a silica component led to an increase in the Rho value of the soil. Indicators of G.Z.i. (R^2 = 0.29; Fig., 14), R.Z.i. (R^2 = 0.13; Fig. 15), and S.A.F. (R^2 = 0.41; Fig., 16) were found to have inadequate models (R^2 0.50), Table (7). On the basis of their electrical resistivity signature, these indices could not accurately predict the weathering process or the source rock in the studied sediments and soils. The findings demonstrated that, the soil's electrical resistivity could successfully classify various soil parameters, which is helpful for both soil management and the comprehension of the condition of the soil parameters. Even though the electrical resistivity approach cannot accurately predict certain soil properties. These parameters can still be classified with a decent level of agreement.

Using the correlation coefficient (r), the results in Table (6) demonstrated that, the soil contents correlated well with the electrical resistivity (Ω·m). The quantitative assessment of soil components using electrical resistivity (Ω·m) is shown in Figs. (7 to 16), with regression analysis revealing the most significant correlation for each soil attribute. The laboratory uses electrical resistivity (Ω·m) to build predictive equations for clay and sand fractions, as shown in Figs. (7 and 8). A substantial negative association with soil organic matter reflects its constituents' qualities. Soil electrical resistance can be used to estimate organic matter

reliably. Rho measurement is one of the simplest methods for acquiring soil information. As a result, soil Rho is now commonly employed to characterize differences in soil parameters. Because the usability of geophysical methods is closely related to various soil parameters and the quantity of undesired "noise" or interference, it is critical to fully understand Rho measurements before using them in any digital soil mapping. Results indicate a precise spatial prediction of root-restrictive layers with soil pedons when top-soil water content and soil bulk density factors are considered in the mapping process. According to the study, new geophysical techniques using soil electrical resistivity have enabled quick prediction, quantification, and mapping of soil parameters, including homogeneity and origin. Ultimately, these strategies help connect sensor data and soil parameters more explicitly. Combining these data sources and other information could lead to precise soil mapping with minimal sampling. It applies to soil resource inventory, conservation management, land evaluation, and sustainable land use planning.

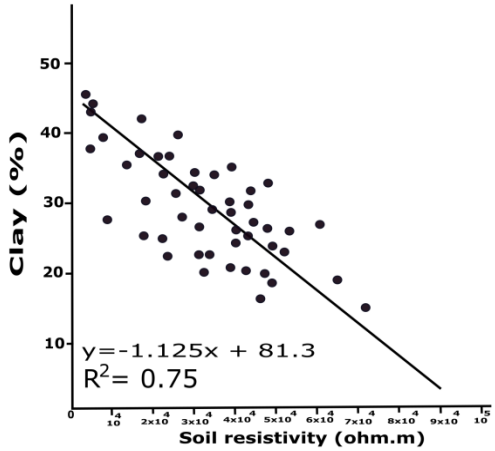

Fig. (7): Linear regression of clay content on soil resistivity (Rho)

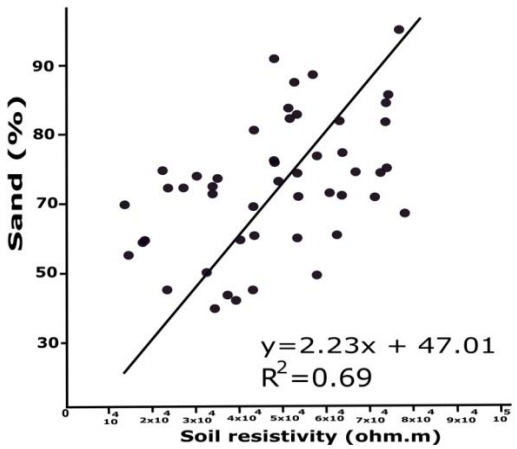

Fig. (8): Linear regression of sand content on soil resistivity (Rho)

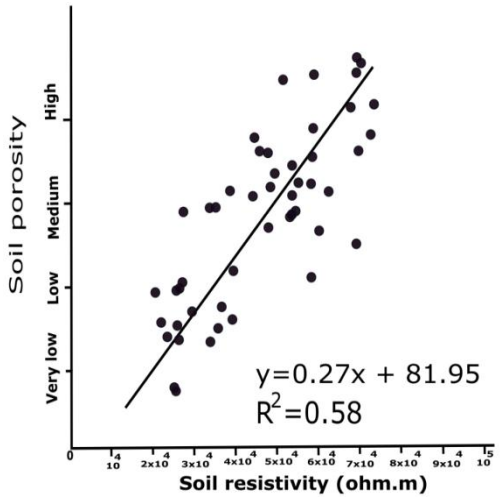

Fig. (9): Linear regression of soil porosity on soil resistivity (Rho)

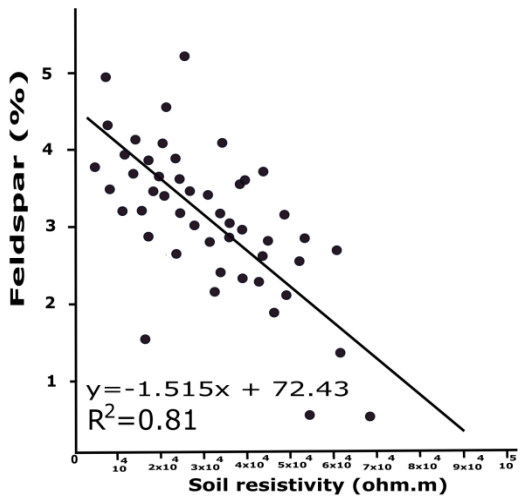

Fig. (10): Linear regression of feldspar on soil resistivity (Rho)

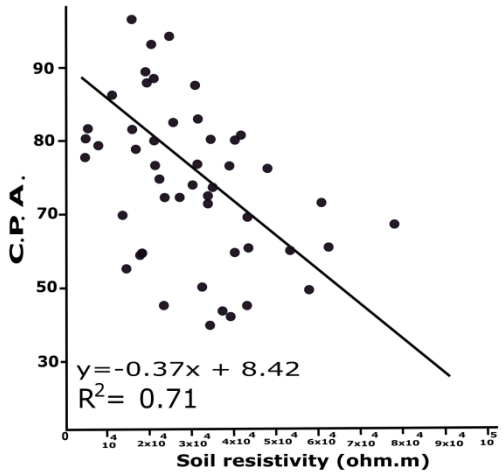

Fig. (11): Linear regression of C.P.A. (Weathering index) on soil resistivity

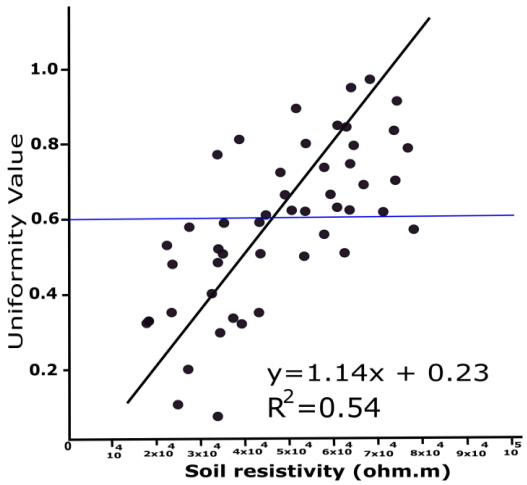

Fig. (12): Linear regression of uniformity value with soil resistivity (Rho)

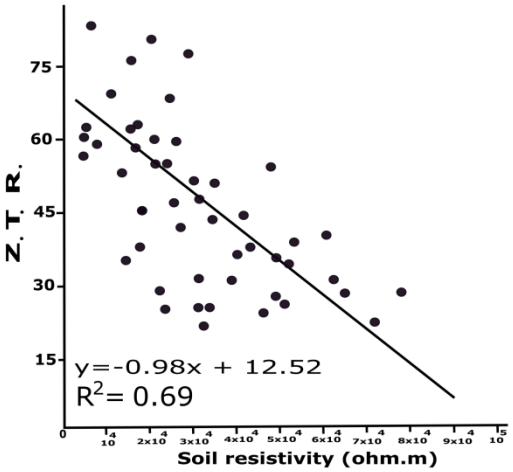

Fig. (13): Linear regression of Z.T.R. on soil resistivity (Rho)

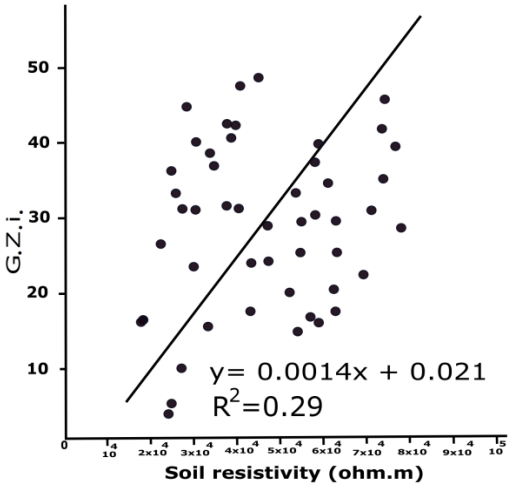

Fig. (14): Linear regression of G.Z.i. on soil resistivity (Rho)

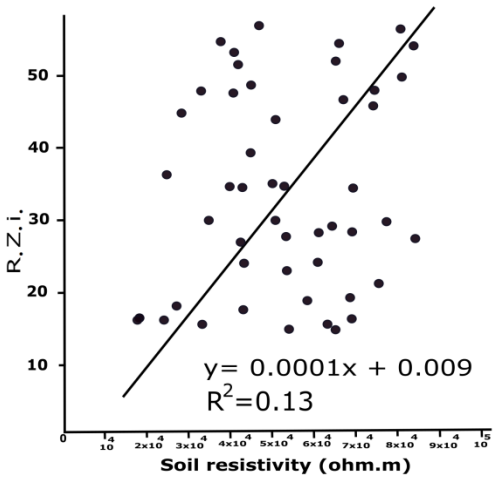

Fig. (15): Linear regression of R.Z.i. index on soil resistivity (Rho)

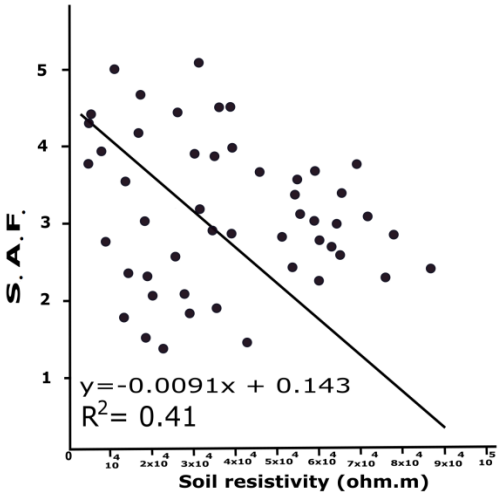

Fig. (16): Linear regression of S.A.F. index on soil resistivity (Rho)

Rho was shown to be substantially linked with soil parameters such as water, clay, homogeneity, maturity, and weathering indices. Electrical current in soils is primarily electrolytic, resulting from ion displacement in pore water. Water quality and quantity in soil pores affect electrical current, as seen in the deepest horizon Btg of P4 at downstream soils. When studying water content, electrical conductivity is often believed to be constant and ignored when considering variations in water content. Findings indicate a strong positive association between Rho and soil porosity across several strata. The relationships between Rho and soil salinity were examined due to the high salt content in soils, such as Btkz in downstream soils.

Similarly, soil temperature remained steady throughout the survey in our study. Numerous correlations between Rho and soil properties at the study site demonstrate the potential for geophysical methods to record and accurately predict soil properties directly. The study found a substantial correlation between soil's apparent resistivity, horizons, root-restrictive layers, porosity, clay, sand, A.W.H.C., Z.T.R. maturity index, C.P.A., and uniformity value index. Rho in standard regressions, effectively identified geographical trends in these attributes.

Insulators make up the vast majority of rock minerals. However, rocks like those found in the Cr and R layers of the P1 at upstream soils can frequently act as electrical conductors. This process is because the pores and crevices in these rocks can keep water in place. The resistivity of groundwater, such as that found in the W zone of P4 at downstream of Wadi El-Madamude, is extremely low. Still, soil resistivity is primarily determined by the soil's porosity and the extent to which the soil's pores are saturated with water. Ionic conduction is the process by which a current is formed when positively charged and negatively charged ions move through water in the opposite direction of one another (Bovi *et al*., 2020). Dissolved salts can dissociate in natural fluids into positive and negative ions, as seen in P4 downstream. Air and other insulating materials differ from conducting ones due to the movement of electrical charges. Soil materials have mid-range electrical properties influenced by physical and chemical factors such as texture, salinity, and water content. Rho depends on soil properties, including solid constituents (particle size distribution, mineralogy), void arrangement (porosity, pore size distribution, connectivity), water saturation (water content), and fluid electrical resistivity (solute concentration).

Additional information on other soil characteristics must be gathered using geophysical techniques to extract relevant information about a soil property. Obtaining extra soil information can be costly, particularly for vast areas with high soil bulk density. Soil water content data can be collected using portable TDR equipment, while bulk density can be measured using indirect methods such as soil penetrometry. Automation is possible for both procedures.

CONCLUSION

This study looked at the relationship between soil electrical resistivity and various soil properties for soil uniformity and origin detection using geophysical methods and pedological criteria. Soil apparent resistivity (Rho) values acquired using a portable resistivity meter were compared to known soil parameters and computed indices based on soil fractions, mineralogical composition, and geochemical measurements. Soil samples were taken from a landscape site across a catena of Wadi El-Madamude in east Luxor, Upper Egypt. In downstream soils, the most significant connections were established between Rho and accessible water content, soil clay content, soil bulk density, and depth to the root-restrictive layers or clayey horizons (Bw, Btkz, Btkm, Btm, Btg). Using the soil's apparent resistivity to predict the geographic variations in soil water content, soil clay content, soil bulk density, depth to the clayey horizon, and Z.T.R. maturity index appeared to be an accurate and successful strategy. However, because Rho may fluctuate geographically and temporally, as may soil water

content at different sites, new statistical correlations would have to be created.

Geophysical techniques record soil property fluctuations and interference from other properties, resulting in unwanted noise that hinders digital soil mapping. This study explores the correlation between soil geophysical characteristics and properties, potentially enhancing geophysical surveys. The study found that integrating Rho with other soil characteristics like bulk density, porosity, clay content, and sand component water content can accurately predict variations in root-restrictive layer thickness, uniformity, and genesis indices. The regression study of Rho and other soil parameters provides a solid foundation for defining a specific soil feature. This method can forecast soil origin and homogeneity using geophysical data, perhaps offering a new perspective on geophysical surveys. Understanding the link between geophysical signals and soil patterns is crucial for accurately mapping specific soil features using geophysical techniques. As the value of soil resources and ecological services is recognized, digital soil mapping using apparent electrical resistivity can provide spatial data on soil degradation, aiding conservation and rehabilitation efforts.

REFERENCES

Ahmed, A.A. (2009). Land Use Change and Deterioration of Pharaonic Monuments in Upper Egypt. Journal of Engineering Science, Assiut University, 37(1): 161 – 177.

Ahmed, A.A. and Fogg, G.E. (2014). The Impact of Groundwater And Agricultural Expansion on The Archaeological Sites at Luxor, Egypt, Journal of African Earth Sciences 95: 93–104.

Bovi, R.C.; Moreira, C.A.; Rosolen, V.S.; Rosa, F.T.G.; Furlan, L.M. and Helene, L.P.I. (2020). Piping process: Genesis and network characterization through a pedological and geophysical approach. Geoderma, 361: 114101.

Buggle, B.; Glaser, B.; Hambach, U.; Gerasimenko, N. and Marković, S. (2011). An evaluation of geochemical weathering indices in loessepaleosol studies. Quat. Int., 240: 12-21.

Burt, R. and Soil Survey Staff (2014). Kellogg Soil Survey Laboratory Methods Manual. Soil Survey Investigations Report No. 42, Version 5.0., Lincoln NE: U.S. Department of Agriculture, Natural Resources Conservation Service .

Cremeens, D. L. and Mokma, D. L. (1986). Argillic horizon expression and classification in the soils of two Michigan hydrosequences. Soil Sci. Soc. Am. J., 50: 1002-1007.

Darmody, R. G.; Thorn, C. E. and Allen, C. E. (2005). Chemical weathering and boulder mantles, Kärkevagge, Swedish Lapland. Geomorphology, 67: 159-170.

Düzgören-Aydin, N. S.; Aydin, A. and Malpas, J. (2002). Re-assessment of chemical weathering indices: case study of pyroclastic rocks of Hong Kong. Eng. Geol., 63: 99-119.

Edouard, S.; Combes, D.; Van Iseghem, M.; Tin, M.N.W. and Escobar-Guti´errez, A.J. (2023). Increasing land productivity with agriphotovoltaics: application to an alfalfa field. Appl Energy;329. https://doi.org/ 10.1016/j.apenergy .2022.120207.

Egyptian Meteorological Authority (2022). Climatic Atlas of Egypt, Cairo, Egypt.

EL Shamy, I. Z.; Gad, M. I.; Shedid, M.; EL Kazzaz, Y.A. and Ammar, M.A. (2013). Flash Flood Estimation in Luxor Area with Emphases on Wadi ElMadamud, South Egypt. Egyptian Journal of Geology, 57: 103-117.

FAO (2006). Guidelines for Soil Description. 4th Edition. Food and Agriculture Organization of the United Nations, Rome, Italy.

Grossman, R.B. and Reinsch, T.G. (2002). The solid phase. In: Dane, J.H., Topp, G.C. (Eds.), Methods of Soil Analyses: Part 4 – Physical Methods. Soil Science Society of America, Wisconsin.

Heidari, A.; Osat, M. and Konyushkova, M. (2022). Geochemical indices as efficient tools for assessing the soil weathering status in relation to soil taxonomic classes. Catena 208: 105716.

Hu, J.; Huang, Z.; Li, S.; Liu, B. and Ci. E. (2023). Assessing profile uniformity of soils from weathered clastic sedimentary rocks in southwest China. Catena 224: 107007.

Hubert, J. F. (1962). A zircon-tourmaline-rutile maturity index and independence of composition of heavy mineral assemblages with gross composition and texture of sandstones. J. Sediment. Petrol., 32: 440-450.

I.U.S.S. Working Group W.R.B. (2022). World Reference Base for Soil Resources. International soil classification system for naming soils and creating legends for soil maps. 4th edition. International Union of Soil Sciences (I.U.S.S.), Vienna, Austria.

Lee, S.; Hyuk Lee, J.; Jeong, Y.; Kim, D.; Hun Seo, B. and Jin Seo, Y. (2023). Agrivoltaic system designing for sustainability and smart farming: Agronomic aspects and design criteria with safety assessment. Appl Energy 2023;341:121130. https://doi.org/ 10.1016/j.apenergy.121130.

Lu, R.K. (2000). Analytical Methods of Agricultural Chemistry in Soil. China Agricultural Scientech Press, Beijing, China.

Mange, M. A. and Maurer, H. F. W. (1992). Heavy minerals in Colour. Chapman and Hall, London, pp. 147.

Mange, M.A. and Wright, D. T. (2007). Heavy Minerals in Use. Developments in Sedimentology, 58, Elsevier, Amsterdam, pp. 1328.

Mani, A.K.; Santhi, R. and Sellamuthu, K.M. (2007). A Handbook of Laboratory Analysis. 1st edition. ISBN: 978-81-902558-8-2, A.E. Publications, Coimbatore, Tamil Nadu, India.

Morton, A. C. and Hallsworth, C. R. (1994). Identifying provenance-specific features of detrital heavy mineral assemblages in sandstones. Sediment. Geol., 90(3-4): 241-256.

Nesbitt, H.W. and Young, G.M. (1982). Early Proterozoic climates and plate motions inferred from major element chemistry of luttites. Nature, 291: 715-717.

Nesbitt, H.W. and Young, G.M. (1984). Prediction of some weathering trends of plutonic and volcanic rocks based on thermodynamic and kinetic considerations. Geochimica et Cosmochimica Acta, 48: 1523-1534.

Rangaswamy, R. (1995). Correlation and regression analysis. A Textbook of Agricultural Statistics. New age international publishers limited Wiley eastern limited, New Delhi, 142-183.

Razum, I.; Rubinić, V.; Miko, S.; Ružičić, S. and Durn, G. (2023). Coherent provenance analysis of terra rossa from the northern Adriatic based on heavy mineral assemblages reveals the emerged Adriatic shelf as the main recurring source of siliciclastic material for their formation. Catena 226: 107083.

RIGW (1997). Hydrogeological maps of Egypt, scale 1:100,000. Water Research Center, Ministry of Public Works and Water Resources, Egypt.

Salman, S.A.; Arauzob, M. and Elnazera, A.A. (2019). Groundwater quality and vulnerability assessment in west Luxor Governorate, Egypt. Groundwater for Sustainable Development 8: 271–280.

Schaetzl, R. J. and Anderson, S. (2005). Soils: Genesis and Geomorphology. Cambridge University Press, Cambridge, p. 817.

Schoeneberger, P.J.; Wysocki, D.A.; Benham, E.C. and Soil Survey Staff (2012). Field book for describing and sampling soils, Version 3.0. Natural Resources Conservation Service, National Soil Survey Center, Lincoln, NE.

Sheldrick, B. H. and Wang, C. (1993). Particle size distribution. p. 499-511. In M.R. Carter (ed.) Soil sampling and methods of analysis. Lewis Publ., Boca Raton, FL.

Soil Science Division Staff (2017). Soil Survey Manual. United States Department of Agriculture (U.S.D.A.), Agriculture Handbook No. 18. Natural Resources Conservation Service, Washington, DC.

Soil Survey Staff (2022). Keys to Soil Taxonomy, 13th edition. U.S.D.A. Natural Resources Conservation Service, Washington, DC.

Tung, C.C. and Lim, S.C. (2017). Performance of electrical grounding system in soil at low moisture content conditions at various compression levels. J. Eng. Sci. Technol. 12: 27–47.

Walter, N. F.; Hallberg, G. R. and Fenton, T. F. (1978). Particle-size analysis by the Iowa State University Soil Survey Laboratory, p. 61-74. In Hallberg G.R. (ed.) Standard procedures for evaluation of Quaternary materials in Iowa. Iowa Geological Survey Technical Information Series Number 8, Iowa City, Iowa.

Wang, D. and Zhu, A. (2020). Soil mapping based on the integration of the similarity-based approach and random forests. Land. 9 (6): 174.

Wilson, M.J. (2019). The importance of parent material in soil classification: A review in a historical context. Catena 182: 10413.

Woodruff, L.; Cannon, W. F.; Smith, D. B. and Solano, F. (2015). The distribution of selected elements and minerals in soil of the conterminous United States. J. Geochem. Explor., 154: 49-60

Ya'acob, M.E.; Lu, L.; Zulkifli, S.A.; Roslan, N. and Wan Ahmad, W.F.H. (2023). Agrivoltaic approach in improving soil resistivity in large scale solar farms for energy sustainability. Applied Energy 352: 121943.

Yang, H. F.; Yang, S. L.; Xu, K. H.; Milliman, H.; Wang, Z.; Yang, Z. Chen and Zhang, C. Y. (2018). Human impacts on sediment in the Yangtze River: A review and new perspectives. Global and Planetary Change, 162: 8-17.

Yang, S. Y.; Li, C. X.; Yang, D. Y. and Li, X. S. (2004). Chemical weathering of the loess deposits in the lower Changjiang Valley, China, and paleoclimatic implications. Quat. Int., 117: 27-34.

Zhu, X.; Fu, S.; Wu, Q. and Wang, A. (2020). Soil detachment capacity of shallow overland flow in Earth-Rocky Mountain Area of Southwest China. Geoderma 361: 114021.

أصل وتجانس التربة في الأحواض المحكومة بالسدود عبر وادي المدامود باستخدام القياسات البيدولوچية والـچيوكهربية، شرق الأقصر، مصر

عادل عبدالحميد علوان خليل[١] ، مصطفى سعيد مصطفى برسيم[٢]

[١] قسم البيدولوچي، مركز بحوث الصحراء، ١ش متحف المطرية، رقم بريدي ١١٧٥٣، القاهرة، مصر

[٢] قسم الاستكشاف الـچيوفيزيائى، مركز بحوث الصحراء، ١ش متحف المطرية، رقم بريدي ١١٧٥٣، القاهرة، مصر

الملخص العربى

تعتبر الأساليب التقليدية المُستخدمة في علوم الأراضي لتقدير التغيرات المكانية لخصائص التربة داخل أي مزرعة من أهم المعوقات التي تستغرق وقتًا وجهداً ومالاً، ولا تسمح بتقييم التغيرات القصيرة المدى. تقدم التقنيات الـچيوفيزيائية Geophysical techniques بديلاً عن أساليب أخذ العينات التقليدية للتربة بدقة عالية. كان الهدف الرئيسي من هذا البحث هو اختبار مدى ملاءمة استخدام قياس المقاومة الكهربائية النوعية للتربة (Rho; ρ) كأحد التقنيات الـچيوفيزيائية من أجل التنبوء بالخصائص المختلفة المتعلقة بأصل التربة وتجانسها عبر قطاعات التربة في وادي المدامود، شرق الأقصر، مصر. ولتنفيذ هذا الهدف، تم إجراء العديد من التحليلات الاحصائية من أجل ربط قيم المقاومة الكهربية النوعية Rho مع العديد من الخصائص المورفولوچية والفيزيائية والكيميائية والمعدنية والـچيوكيميائية للتربة. تم قياس المقاومة النوعية معملياً لعينات التربة والممثلة للطبقات والآفاق البيدوجينية لقطاعات التربة الممثلة لأنواع الأراضي بوادي المدامود، شرق محافظة الأقصر، جنوب مصر. كما أنه تم تصنيف أراضي وادي المدامود إلى أربع مجموعات تربة مرجعية RSGs بناءً على نظام W.R.B. وهي: Leptosols ، Regosols، Calcisols و Solonchaks ، وكان أهم التتابعات الطبقية والأفقية للقطاعات المدروسة طبقا لكل نوع تربة من upstream إلى downstream كالتالي: C-Cr-R لـ Leptosols ، C-Ck-2Cm-Cr لـ Regosols، Ap-Bk-2Ck1-2Ck2 لـ Calcisols ، و Ap-Bw-Btkz-Btkm-Btm-Btg-W لـ Solonchaks. ، وأوضحت نتائج الدراسة الاختلاف الكبير والواضح بين قيم Rho سواء أفقياً عبر وادي المدامود أو رأسياً داخل الطبقات الأرضية لقطاع التربة. كما تتمتع التربة الطينية لـ Solonchaks بقيم مقاومة أقل من التربة الرملية لـ Leptosols و Regosolsحيث تتفاوت القيم طبقاً لنوع التربة فنجد أراضي Leptosols تمتلك أعلى القيم (٩٨١٢٠.٥-٧٠١٢٩.٣ أوم متر) كذلك أراضي Regosols (13546.1-59147.5 أوم متر) بينما قلت القيم في أنواع الأراضي الأخرى فسجلت بأراضي Calcisols (7126.3-21357.2 أوم متر) ، وقلت تماماً في أراضي Solonchaks (55.1-73.2 أوم متر). تم تقييم التربة لأصلها وتجانسها على أساس الدراسات المعدنية والجيوكيميائية ومؤشرات وأدلة التجوية ونضج التربة. وتكونت معظم رواسب upstream و downstream لوادي المدامود من المصادر المختلطة من الحجر الجيري والصخور المتحولة عالية الدرجة، بينما أراضي downstream تكونت من خليط رواسب السهول الفيضية النيلية ناعمة القوام مع رواسب الوديان الخشنة الأحدث التي تأتي من المناطق الجبلية (upstream و downstream). وتم اكتشاف Lithologic discontinuities داخل قطاعات التربة والممثلة لأراضي Calcisols و Regosols . تم تحديد تجانس التربة باستخدام قيمة التجانس Uniformity value و معامل الانحراف المعياري لنسب Ti/Zr و sand/silt . تم استخدام مؤشرات ZTR و CPA لتقييم نضج التربة ومعدلات التجوية. تم ربط هذه المؤشرات وخصائص التربة الأخرى بـ Rho باستخدام التحليل الإحصائي كمحاولة لتحديد تجانس وأصل التربة باستخدام التقنية الجيوفيزيائية. تُظهر درجة الإرتباط بين Rho وخصائص التربة في موقع الدراسة بوادي المدامود أن النهج الجيوفيزيائي بإستخدام تقنية المقاومة الكهربية النوعية يمكن أن يتنبأ بشكل موثوق ويسجل تغيرات خصائص التربة المختلفة . وقد أظهرت نتائج الدراسة أن Rho كانت لها علاقة قوية مع تكون الأفق الملحي خلال قطاعا التربة مسبباً مُحد لنمو الجذور (r=-0.91) ، وطبقة lithic bedrock (r=0.92) ، والمسامية (r=0.89) ، ومحتوى الطين (r=-0.79)، والرمل(r=0.62) ، والكثافة الظاهرية (BD) ، وقدرة التربة على الاحتفاظ بالماء المتاح (AWHC) ، وغيرها من صفات التربة ، بالاضافة إلى دليل نضج رواسب التربة ZTR (r=-0.78) ، ودليل CPA للتجوية (r=-0.74)، وقيمة التجانس (UV) (r=0.87) ، وكما وأظهرت منحنيات الانحدارات القياسية regression curves بين المقاومة النوعية للتربة Rho وخصائص التربة المختلفة قدرة الطرق الجيوفيزيائية بدقة عالية على قياس وتنبؤ بمنشأ التربة وتقييم درجة تجانسها.